J. Phys. A: Math. Theor. **45** (2012) 415309 (28pp) doi:10.1088/1751-8113/45/41/415309

Restricted numerical shadow and the geometry of quantum entanglement

Zbigniew Puchała[1], Jarosław Adam Miszczak[1], Piotr Gawron[1], Charles F Dunkl[2], John A Holbrook[3] and Karol Życzkowski[4,5]

[1] Institute of Theoretical and Applied Informatics, Polish Academy of Sciences, Bałtycka 5, 44-100 Gliwice, Poland
[2] Department of Mathematics, University of Virginia, Charlottesville, VA 22904-4137, USA
[3] Department of Mathematics and Statistics, University of Guelph, Guelph, Ontario N1G 2W1, Canada
[4] Instytut Fizyki im Smoluchowskiego, Uniwersytet Jagielloński, Reymonta 4, 30-059 Kraków, Poland
[5] Centrum Fizyki Teoretycznej, Polska Akademia Nauk, Aleja Lotników 32/44, 02-668 Warszawa, Poland

E-mail: z.puchala@iitis.pl, miszczak@iitis.pl, gawron@iitis.pl, cfd5z@virginia.edu, jholbroo@uoguelph.ca and karol@tatry.if.uj.edu.pl

Received 8 May 2012, in final form 6 September 2012
Published 2 October 2012
Online at stacks.iop.org/JPhysA/45/415309

Abstract

The restricted numerical range $W_R(A)$ of an operator A acting on a D-dimensional Hilbert space is defined as a set of all possible expectation values of this operator among pure states which belong to a certain subset R of the set of pure quantum states of dimension D. One considers for instance the set of real states, or in the case of composite spaces, the set of product states and the set of maximally entangled states. Combining the operator theory with a probabilistic approach we introduce the restricted numerical shadow of A—a normalized probability distribution on the complex plane supported in $W_R(A)$. Its value at point $z \in \mathbb{C}$ is equal to the probability that the expectation value $\langle\psi|A|\psi\rangle$ is equal to z, where $|\psi\rangle$ represents a random quantum state in subset R distributed according to the natural measure on this set, induced by the unitarily invariant Fubini–Study measure. Studying restricted shadows of operators of a fixed size $D = N_A N_B$ we analyse the geometry of sets of separable and maximally entangled states of the $N_A \times N_B$ composite quantum system. Investigating trajectories formed by evolving quantum states projected into the plane of the shadow, we study the dynamics of quantum entanglement. A similar analysis extended for operators on $D = 2^3$-dimensional Hilbert space allows us to investigate the structure of the orbits of GHZ and W quantum states of a three-qubit system.

PACS numbers: 03.67.Ac, 02.10.−v, 02.30.Tb

(Some figures may appear in colour only in the online journal)

1. Introduction

Recent studies on quantum entanglement, a crucial resource in the theory of quantum information processing, contributed a lot to our understanding of this deeply non-classical phenomenon (see e.g. [1] and references therein). In particular, some progress has been achieved in elucidating the geometry of quantum entanglement [2–7], but several questions concerning this topic remain still open [8–10]. It was also suggested that a geometric approach is useful to classify and quantify quantum entanglement [8, 11, 12].

The phenomenon of quantum entanglement, non-classical correlations between individual subsystems, may arise in composite physical systems. Consider then the simplest composite system, which consists of two parts and can be described in a Hilbert space with a tensor product structure, $\mathcal{H}_D = \mathcal{H}_A \otimes \mathcal{H}_B = \mathcal{H}_{N_A} \otimes \mathcal{H}_{N_B}$. Any product pure state, $|\psi\rangle = |\phi_A\rangle \otimes |\phi_B\rangle$, is called *separable*, while all other pure states are called *entangled*. The set $\mathcal{S}$ of all separable pure states has the structure of the Cartesian product of the complex projective spaces [8], $\mathcal{S} = \mathbb{C}\mathbf{P}^{N_A-1} \times \mathbb{C}\mathbf{P}^{N_B-1}$.

Among entangled pure states of a bipartite system, one distinguishes the set $\mathcal{E}$ of *maximally entangled* states, such that the partial trace of the corresponding projector is proportional to the identity matrix. The set $\mathcal{E}$ contains the generalized Bell state, $|\psi_+\rangle = \frac{1}{\sqrt{N}} \sum_i |i, i\rangle$, and all states obtained from it by a local unitary transformation, $U_A \otimes U_B |\psi_+\rangle \in \mathcal{E}$. The set of maximally entangled states is thus equivalent to $\mathrm{U}(N)/\mathrm{U}(1)$. The structure of the set $\mathcal{E}$ and other sets of locally equivalent entangled states of a bipartite system was studied in [13].

In this work we propose to analyse the geometry of the set of entangled and separable quantum states using the algebraic concepts of the numerical range and numerical shadow of an operator. For any operator A acting on the complex Hilbert space $\mathcal{H}_D$, one defines its *numerical range* [14, 15] as a subset of the complex plane which contains expectation values of A among arbitrary normalized pure states

$$W(A) = \{z : z = \langle\psi|A|\psi\rangle, |\psi\rangle \in \mathcal{H}_D, \ \langle\psi|\psi\rangle = 1\}. \tag{1}$$

Due to the classical Toeplitz–Hausdorff theorem, the set $W(A)$ is convex—see e.g. [16]. The differential topology and projection aspects of numerical range were investigated in [17, 18].

The standard notion of numerical range, often used in the theory of quantum information [19–21], can be generalized in several ways [22–24]. For instance, for an operator acting on a composite Hilbert space, one defines the *product* numerical range [25] (also called *local* numerical range [24]) and a more general class of numerical ranges *restricted* to a specific class of states [21]

$$W_R(A) = \{z : z = \langle\psi|A|\psi\rangle, \ |\psi\rangle \in R \subset \Omega_D, \ \langle\psi|\psi\rangle = 1\}. \tag{2}$$

Here $R \subset \Omega_D$ denotes a selected subset of the set of pure quantum states of a given size D. For instance, one may consider the set of all real states, or, in the case of composite spaces, the set of complex product states or the set of real maximally entangled states.

For any operator A acting on $\mathcal{H}_D$, one defines a probability density $P_A(z)$ on the complex plane [26, 27], supported in the numerical range $W(A)$,

$$P_A(z) \ := \int_{\Omega_D} \mathrm{d}\mu(\psi) \, \delta(z - \langle\psi|A|\psi\rangle). \tag{3}$$

Here $\mu(\psi)$ denotes the unique unitarily invariant measure on the set Ω_D of D-dimensional quantum pure states, also called Fubini–Study (FS) measure. In other words the shadow of A at a given point $z \in \mathbb{C}$ characterizes the likelihood that the expectation of A among a random pure states is equal to z. Sometimes it is convenient to treat the numerical shadow as a probability measure μ_A, on a complex plane. For any measurable set E it reads $\mu_A(E) = \mu(\{\psi : \langle\psi|A|\psi\rangle \in E\})$.

If the operator A is normal, $AA^\dagger = A^\dagger A$, its shadow $P_A(z)$ can be interpreted as a projection of the set of classical states—the D-dimensional regular simplex of probability distributions—into a two plane [28]. In the more general case of a non-normal A, its shadow can be associated with a probability distribution obtained by projecting the set Ω_D of quantum pure states of size D into a plane. Thus choosing a matrix A to be analysed, one fixes the relative position of the set Ω_D and determines the direction, along which it is the projection on the plane. Hence investigating all possible shadows of various operators of a given size D, one gathers information about the structure of the set Ω_D.

Combining the ideas of the restricted numerical range (2) with the numerical shadow (3), one is led in a natural way to the definition of a *restricted numerical shadow*

$$P_A^R(z) := \int_R \mathrm{d}\mu(\psi)\, \delta(z - \langle\psi|A|\psi\rangle), \tag{4}$$

where R is the selected subset of Ω_D. In particular, choosing the appropriate subsets of the set of pure states we define the numerical shadow restricted to *real* states or SU(2)-coherent states. In the case of a composite Hilbert space one defines the shadow with respect to *separable* states or *maximally entangled* states. The restrictions can be combined, so one can consider the shadow restricted e.g. to real separable states, or in the case of operators acting on an eight-dimensional space, which describes a three-qubit system, one may study the shadow with respect to real GHZ states or complex W states. It will be convenient to use simplified terms, so for brevity we will slightly abuse the notation and write about the 'separable shadow', 'real entangled shadow' or 'complex GHZ shadow' of a given operator. Using the notion of probability measure we will denote this restriction by μ_A^R.

On the one hand, for a given matrix A one may study its restricted numerical shadows $P_A^R(z)$ determined by a given set R of quantum states. Alternatively, investigating numerical shadows of various matrices of a fixed dimension D with respect to a concrete subset $R \in \Omega_D$, one may analyse its geometry. In this work we study in this way the structure of the set of real, separable and maximally entangled quantum states for a two- and three-qubit system.

The rest of this paper is organized as follows. In section 2 some basic properties of the numerical range and the numerical shadow are reviewed. In section 3 we discuss the numerical shadow restricted to real states. In the case of operators acting on the Hilbert space with a tensor product structure, $\mathcal{H} = \mathcal{H}_N \otimes \mathcal{H}_N$, one defines classes of separable and maximally entangled states. Numerical ranges restricted to these sets are analysed in sections 4 and 5, respectively. In section 6 we show that investigations of trajectories formed by evolving quantum states projected into the plane of the shadow contribute to understanding the dynamics of quantum entanglement. In section 7 we discuss the simplest case of a composite system that consists of three parts and describe in the Hilbert space $\mathcal{H}_8 = \mathcal{H}_2 \otimes \mathcal{H}_2 \otimes \mathcal{H}_2$. In the set Ω_8 of pure states acting on this space, one defines two classes of entangled states called GHZ and W. For any operator acting on $\mathcal{H}_8$ it is then natural to introduce the shadow restricted to states locally equivalent to GHZ or W, and these are investigated in section 6.

2. Standard numerical shadow and the geometry of quantum states

2.1. Classical and quantum states

Elements of a Hilbert space are used as basic objects of the quantum theory. A physical system with D distinguishable states can be described by an element $|\psi\rangle$ of the complex Hilbert space $\mathcal{H}_D$. It is assumed that such a *pure quantum state* is normalized, $||\psi||^2 = \langle\psi|\psi\rangle = 1$, so it belongs to the hypersphere of dimension $2D - 1$. One identifies any two states, which differ

only by a global phase, $|\psi\rangle \sim |\phi\rangle = \mathrm{e}^{\mathrm{i}\alpha}|\psi\rangle$. The set of all pure quantum states Ω_D acting on $\mathcal{H}_D$ is therefore equivalent to the complex projective space, $\Omega_D = \mathbb{C}\mathbf{P}^{D-1}$ (see e.g. [8]).

Any convex combination of projectors onto pure states forms a *mixed quantum state*, $\rho = \sum_i p_i|\psi_i\rangle\langle\psi_i|$ with $p_i \geqslant 0$ and $\sum_i p_i = 1$. Any such state ρ, also called a density operator, is Hermitian, positive and normalized by the trace condition, $\mathrm{Tr}\rho = 1$. Thus the set $\mathcal{Q}_D$ of all density matrices of order D forms a convex set of $D^2 - 1$ real dimensions. The projectors corresponding to the extremal points of the set of density operators form the set of pure quantum states, $\Omega_D = \mathbb{C}\mathbf{P}^{D-1} \subset \mathcal{Q}_D$. In the one-qubit case, $D = 2$, the set of pure quantum states forms the *Bloch sphere*, $\Omega_2 = \mathbb{C}\mathbf{P}^1$, which in this case is equivalent to the boundary of the Bloch ball $\mathcal{Q}_2$. For a larger dimension the $(2D - 2)$-dimensional set of pure states Ω_D forms only a zero-measure subset of the $(D^2 - 2)$-dimensional boundary of the set $\mathcal{Q}_D$.

Note that the definitions of the set of pure and mixed quantum states are unitarily invariant, so they can be formulated without specifying any basis in the Hilbert space. On the other hand, among quantum states, one distinguishes also the set of *classical states*, which are formed by the density matrices diagonal in a certain basis. Hence any classical state p is represented by a normalized probability vector, $p = \{x_1, x_2, \ldots, x_D\}$ such that $x_i \geqslant 0$ and $\sum_{i=1}^D x_i = 1$. The set of classical states forms thus the probability simplex $\Delta_{D-1} \subset \mathbb{R}^{D-1}$. Each of the D corners of the simplex represents a classical pure state, and their convex hull is equivalent to Δ_{D-1}. In the one-qubit case, $D = 2$, the set Δ_1 of classical states forms an interval which joins two poles of the Bloch sphere and traverses across the interior of the Bloch ball of one-qubit mixed quantum states.

2.2. Numerical range and the set of quantum states

The definition (1) of the numerical range of a matrix A of order D specifies $W(A)$ as the set of expectation values $\langle\psi|A|\psi\rangle$ for normalized pure states $|\psi\rangle$. In fact the compact set $W(A)$ in the complex plane can be considered as a *projection* of the set $\mathcal{Q}_D$ of quantum states onto a two plane. The following facts were recently established in [28].

Proposition 1. *Consider the set of classical states of size D, which forms the regular simplex Δ_{D-1} in $\mathbb{R}^{D-1}$. Then for each normal matrix A of dimension D there exists an affine rank-2 projection P of the set Δ_{D-1} whose image is congruent to the numerical range $W(A)$ of the matrix A. Conversely for each rank-2 projection P there exists a normal matrix A whose numerical range $W(A)$ is congruent to image of Δ_{D-1} under projection P.*

Proposition 2. *Let $\mathcal{Q}_D$ denote the set of quantum states of dimension D embedded in $\mathbb{R}^{D^2-1}$ with respect to Euclidean geometry induced by the Hilbert–Schmidt distance. Then for each (arbitrary) matrix A of dimension D there exists an affine rank-2 projection P of the set $\mathcal{Q}_D$ whose image is congruent to the numerical range $W(A)$ of the matrix A. Conversely for each rank-2 projection P there exists a matrix A whose numerical range $W(A)$ is congruent to image of $\mathcal{Q}_D$ under projection P.*

Thus by fixing the dimension D and selecting various operators A of this order and analysing their numerical ranges $W(A)$, we may gather information about the projections of the set of quantum states. For instance, for $D = 2$ the projections of the Bloch sphere form ellipses (which could form circles or may reduce intervals), and so the numerical range of any operator A of size $D = 2$ may be the result. Similarly the numerical range of operators of size $D = 3$ can be viewed as projections of the set $\Omega_3 = \mathbb{C}\mathbf{P}^2$ of single-qutrit quantum states, while the numerical range for matrices of order $D = 4$ can be associated with projections of the set $\Omega_4 = \mathbb{C}\mathbf{P}^3$ [26, 28].

2.3. Measure on the space of quantum states and the numerical shadow

The Haar measure on the unitary group $\mathrm{U}(D)$ induces on the set Ω_D of quantum pure states the unitarily invariant FS measure μ. In the simplest case of $D = 2$ this measure corresponds to the uniform distribution of points on the Bloch sphere $\Omega_2 = \mathbf{S}^2$.

For any operator A of size D we may compute its expectation value for random pure state $|\psi\rangle \in \Omega_D$ chosen with respect to measure μ. In this way for any operator A we define its *numerical shadow*—a probability distribution (3) on the complex plane. Note that by construction the numerical shadow $P_A(z)$ is supported on the numerical range $W(A)$. Furthermore, the numerical shadow is unitarily invariant: $P_A(z) = P_{UAU^\dagger}(z)$.

For any normal matrix A, which commutes with its adjoint, the numerical shadow $P_A(z)$ covers the numerical range $W(A)$ with the probability corresponding to a projection of a regular simplex Δ_{D-1} of classical states embedded in $\mathbb{R}^{D-1}$ onto a plane. In general, for a non-normal operator A acting on $\mathcal{H}_D$, its shadow covers the numerical range $W(A)$ with the probability corresponding to an orthogonal projection of the complex projective manifold $\Omega_D = \mathbb{C}\mathbf{P}^{D-1}$ onto a plane.

In this work we will analyse the numerical range restricted [21] to a certain subset R of pure quantum states and the corresponding *restricted* numerical shadows, with probability density determined by random states distributed on the subset R according to the measure induced by the FS measure on Ω_D.

2.4. Standard numerical shadow for a diagonal matrix

Consider a diagonal matrix of size D, namely $X = \mathrm{diag}(x_1, \ldots, x_D)$. Let $|1\rangle$ be an arbitrary fixed pure state in $\mathcal{H}_D$. Then the entire set of random pure states can be obtained as $|\psi\rangle = U|1\rangle$, where $U \in \mathrm{U}(D)$ is a random unitary matrix distributed according to the Haar measure. Thus the expansion coefficients of the state $|\psi\rangle$ read $(U_{11}, U_{12}, \ldots, U_{1D})$.

The *numerical shadow* of the operator X is defined as the density distribution of random numbers $z := \langle\psi|X|\psi\rangle$, where $|\psi\rangle$ is a random state defined by the random unitary matrix U. Therefore

$$z := \langle 1|U^\dagger X U|1\rangle = \sum_{i=1}^{D} x_i |U_{1i}|^2 = x \cdot q. \tag{5}$$

Note that the vector of coefficients $q = q_1, \ldots, q_D$ with $q_i = |U_{ij}|^2$ belongs to the $(D-1)$-dimensional simplex Δ_{D-1}. So the complex random variable z can be treated as a scalar product, $z = x \cdot q$, where the complex vector x is given by the diagonal of the operator X, while the probability vector q is random. Its distribution inside the simplex depends on the distribution in the space of unitary matrices $\mathrm{U}(D)$. In cases of interest for us this distribution belongs to the class of *Dirichlet distributions* parametrized by a real number s,

$$P_s(q) \;\propto\; \delta\left(\sum_{i=1}^{D} q_i - 1\right)(q_1 q_2 \ldots q_D)^{s-1}. \tag{6}$$

In particular, we are interested in two situations.

(A) *Standard (complex) numerical shadow* [26, 28], generated by the Haar measure on $\mathrm{U}(D)$. Then the vector q is distributed uniformly with respect to the flat (Lebesgue) measure on Δ_{D-1}, i.e. the Dirichlet measure with the Dirichlet parameter $s = 1$ [8].

(B) *Real* numerical shadow, generated by the Haar measure on the group $\mathrm{O}(N)$ of orthogonal matrices. Then the vector p is distributed with respect to the *statistical measure*, $P_{1/2}(q) \propto 1/\sqrt{q_1 \ldots q_D}$, i.e. the Dirichlet measure with the Dirichlet parameter $s = 1/2$.

In both cases the shadow covers the entire numerical range of X, equal to the convex hull of the spectrum $\{x_i\}_{i=1}^{D}$ with a density determined by the appropriate Dirichlet distribution. The case of real numerical shadow, i.e. the shadow with respect to the real pure states is treated in more detail in the subsequent section.

3. Numerical shadow with respect to real states

Quantum states belonging to a complex Hilbert space form a standard tool of the quantum theory. However, in some cases it is instructive to restrict attention to real states only. On the one hand the set of the real states is easier to analyse than the full set of complex states of larger dimensionality. For instance, the phenomenon of quantum entanglement can be studied for the case of real states of a four-level system, sometimes referred to as a pair of rebits (i.e. real bits) [29].

On the other hand are some physical applications; it is easier to use real orthogonal rotation matrices to construct elements of the entire set of real density matrices. Therefore in this section we will study the shadow of an operator with respect to the set of quantum states with real coefficients. Such an investigation allows us to improve understanding of the structure of the set of real mixed states and its natural subsets.

3.1. Real shadow of operators of size $D = 2$–4

Consider the subset of pure quantum states of size D, that can be represented by real expansion coefficients in a given basis. This set forms a $(D-1)$-dimensional real projective space $\mathbb{R}\mathbf{P}^{D-1} \subset \mathbb{C}\mathbf{P}^{D-1}$.

Substituting into the definition (2) of a restricted numerical range [19, 21] the set $\mathbb{R}\mathbf{P}^{D-1} \subset \mathbb{C}\mathbf{P}^{D-1}$ as the subset R of Ω_D, we arrive at the numerical range restricted to real states. In general the restricted numerical range needs not to be convex or simply connected. Similarly, restricting the integration in (4) to the set $\mathbb{R}\mathbf{P}^{D-1}$ of real quantum states, we obtain the shadow of the operator A with respect to real states. For brevity we will also use a shorter expression, the *real shadow* of A.

In the case of $D = 2$ the set of real states forms the real projective space equivalent to a circle, $\mathbb{R}\mathbf{P}^1 \sim \mathbf{S}^1$. Thus the real shadow of a generic, non-normal matrix of size 2 forms a singular probability distribution supported on an ellipse in the complex plane, and not inside its interior.

The real shadows presented in figure 1 are obtained for illustrative operators of size $D = 2$

$$A_2 = \begin{bmatrix} -1 & 1-\mathrm{i} \\ -\mathrm{i} & 1 \end{bmatrix}, \tag{7}$$

$D = 3$,

$$A_{3a} = \begin{bmatrix} 0 & 1 & 1 \\ 0 & 1 & 1 \\ 0 & 0 & 2 \end{bmatrix}, \quad A_{3b} = \begin{bmatrix} 0 & 1 & 0 \\ 0 & 1 & 0 \\ 0 & 0 & 2\mathrm{i} \end{bmatrix}, \tag{8}$$

and $D = 4$

$$A_{4a} = \begin{bmatrix} 0 & 1 & 1 & 1 \\ 0 & 1 & 1 & 1 \\ 0 & 0 & 2 & 1 \\ 0 & 0 & 0 & 3 \end{bmatrix}, \quad A_{4b} = \begin{bmatrix} 0 & 1 & 1 & 1 \\ 0 & 1 & 1 & 1 \\ 0 & 0 & \mathrm{i} & 1 \\ 0 & 0 & 0 & 1+\mathrm{i} \end{bmatrix}. \tag{9}$$

These probability distributions can be thus interpreted as shadows of real projective spaces $\mathbb{R}\mathbf{P}^2$, $\mathbb{R}\mathbf{P}^3$ and $\mathbb{R}\mathbf{P}^4$ on a plane. In figures 1(*b*) and (*d*) the shadow is supported on a real line,

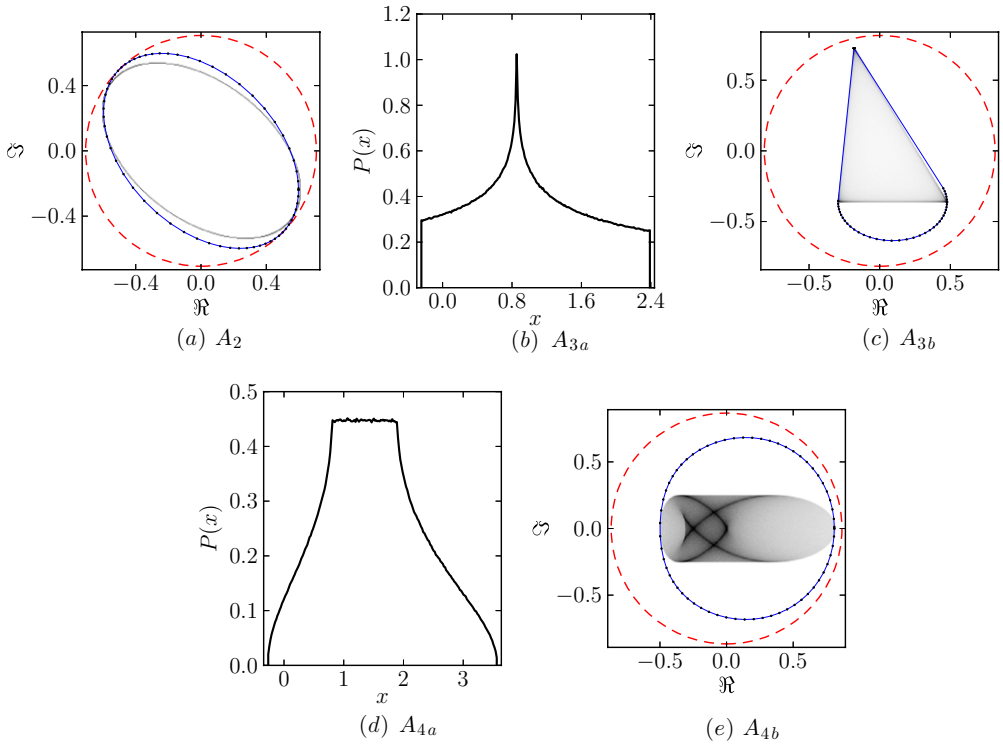

Figure 1. Numerical shadow with respect to real states of illustrative operator of size $D = 2$—panel (*a*) represents projection onto the plane of real projective space $\mathbb{R}\mathbf{P}^2$, $D = 3$—panels (*b*) and (*c*) represent projections onto the plane of real projective space $\mathbb{R}\mathbf{P}^3$, while the real shadows of operators of $D = 4$; panels (*d*) and (*e*) represent projections of real projective space $\mathbb{R}\mathbf{P}^4$. Dashed circles represent the image of the outsphere in which the set of quantum states is inscribed, while dotted lines denote the standard numerical range. Plots (*a*), (*c*) and (*e*) are drawn for matrices translated in such a way that their traces are equal to zero and suitably rescaled as described in [28]. (*a*) A_2, (*b*) A_{3a}, (*c*) A_{3b}, (*d*) A_{4a} and (*e*) A_{4b}.

so we plot the corresponding probability distribution $P_A^{\mathbb{R}}(x)$. In figures 1(*a*), (*c*) and (*e*) the real shadow is supported on the complex plane, so the density is encoded in the greyscale. The circle drawn by the red dashed line represents the image of the sphere of dimension $D^2 - 1$, in which the set of quantum states can be inscribed. The blue dotted line represents the boundary of the standard numerical range of an operator. The restricted shadow is supported in this set or its subset.

The numerical shadow carries also some information about the higher rank numerical range [30, 31] of an operator. For instance, the darker area of the shadow corresponding to a larger probability [28] allows one to recognize in figure 2 the *numerical range of rank 2*, written $\Lambda_2(U)$ of selected unitary matrices. In the case of $D = 4$ shown in figure 2(*a*), it is equal to a single point at which the two diagonals of the quadrangle cross, while for the case $D = 5$ shown in panel (b) the numerical range of rank 2 is represented by the inner pentagon located inside the numerical range; in this case, numerical shadow appears to be uniform in the set $\Lambda_2(U_5)$. In the case $D = 7$ shown in panel (*c*), one can see darker areas between segments connecting every other eigenvalue.

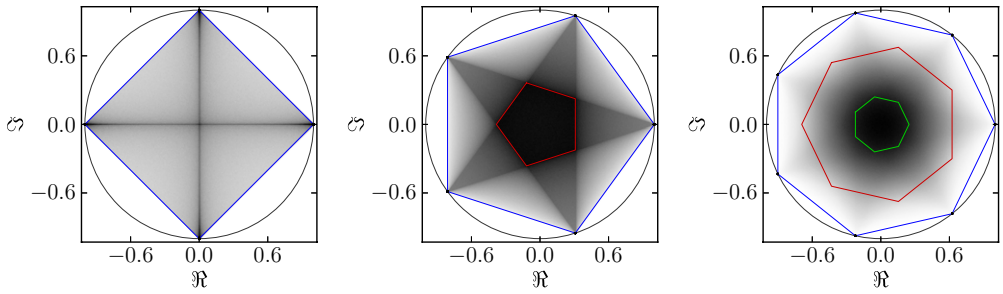

(*a*) diag $\left(\left\{e^{2\pi \mathrm{i}k/4}\right\}_{k=1}^{4}\right)$ (*b*) diag $\left(\left\{e^{2\pi \mathrm{i}k/5}\right\}_{k=1}^{5}\right)$ (*c*) diag $\left(\left\{e^{2\pi \mathrm{i}k/7}\right\}_{k=1}^{7}\right)$

Figure 2. Real shadows of diagonal unitary matrices U of size D having eigenvalues evenly distributed on the unit circle. (*a*) $D = 4$, (*b*) $D = 5$ and (*c*) $D = 7$. The shadow is supported in the regular polygon—the numerical range $\Lambda_1(U) = W(U)$. Inner polygons represent higher order numerical ranges $\Lambda_2(U)$ and $\Lambda_3(U)$. (*a*) diag($\{\mathrm{e}^{2\pi \mathrm{i}k/4}\}_{k=1}^{4}$), (*b*) diag($\{\mathrm{e}^{2\pi \mathrm{i}k/5}\}_{k=1}^{5}$) and (*c*) diag($\{\mathrm{e}^{2\pi \mathrm{i}k/7}\}_{k=1}^{7}$).

3.2. A general approach to the real shadow

Given $M \in M_N(\mathbb{C})$, the real shadow is taken to mean the distribution of (Mx, x) when $x \in \mathbb{R}^N$ is a unit vector randomly chosen from the uniform distribution on $S^{N-1} = \{x \in \mathbb{R}^N : \|x\| = 1\}$.

If M itself is real, we have $(Mx, x) = (x, Mx)$ so that the distribution of (Mx, x) is the same as that of the symmetric $(M + M^T)/2$. Since the uniform distribution on S^{N-1} is invariant under orthogonal transformations, we are free to diagonalize this symmetric matrix. In other words, the real shadow of $M \in M_N(\mathbb{R})$ is that of $\mathrm{diag}(a_1, \ldots, a_N)$, where a_k are the (real) eigenvalues of $(M + M^T)/2$. Thus we need the distribution of

$$\sum_{k=1}^{N} a_k x_k^2. \tag{10}$$

It is known that x uniform on S^{N-1} implies that $p = (x_1^2, \ldots, x_n^2)$ has a Dirichlet-(1/2) distribution on the simplex $\Delta_{N-1} = \{p \in [0, 1]^N : \sum_1^N p_k = 1\}$, i.e. its density is proportional to $1/\sqrt{p_1 p_2 \ldots p_N}$.

The distribution of (10) is known in general [36], so for $a_N < a_{N-1} < \cdots < a_1$ we have

$$\mathrm{Prob}\left(\sum_{k=1}^{N} a_k x_k^2 \leqslant t\right) = \frac{1}{2} - \frac{1}{\pi}\int_0^\infty \frac{\sin\left[\frac{1}{2}\sum_{j=1}^{N} \tan^{-1}\left((a_j - t)u\right)\right]}{u\prod_{j=1}^{N}[1 + (a_j - t)^2 u^2]^{\frac{1}{4}}}\,\mathrm{d}u. \tag{11}$$

As an example, let us consider the Jordan nilpotent $J_3 = \begin{pmatrix} 0 & 1 & 0 \\ 0 & 0 & 1 \\ 0 & 0 & 0 \end{pmatrix}$. For the real shadow of J_3, we first note that it is the same as that of $\mathrm{diag}(1/\sqrt{2}, 0, -1/\sqrt{2})$. Rescaling for convenience, we compute the real shadow of $\mathrm{diag}(1, 0, -1)$. The density $g_3(t)$ of $p_1 - p_3$ is 0 outside $[-1, 1]$, satisfies $g_3(-t) = g_3(t)$, and, in view of the Dirichlet-(1/2) distribution on Δ_2, $g_3(t)$ is proportional to

$$\int_0^{\frac{1-t}{2}} \frac{\mathrm{d}x}{\sqrt{(x + t)(1 - t - 2x)x}}, \tag{12}$$

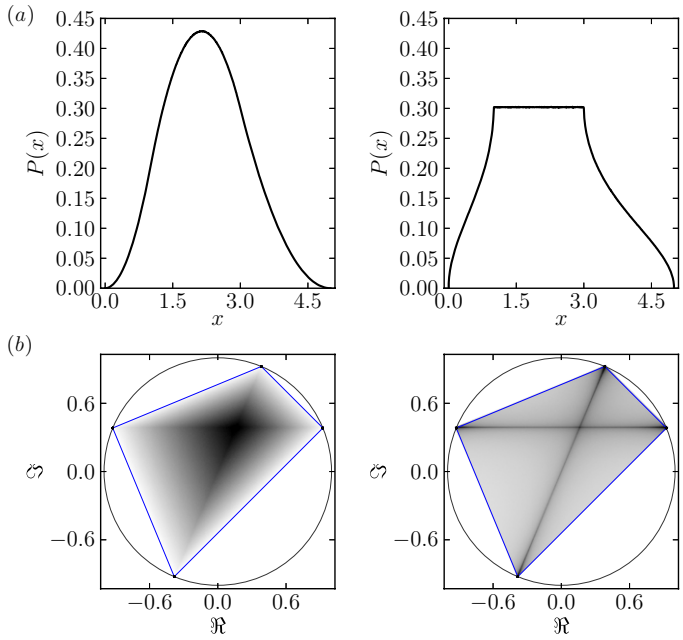

Figure 3. Comparison of real and complex numerical shadows for Hermitian (panel (*a*)) and unitary (panel (*b*)) matrices. (*a*) Complex shadow (left plot) and real shadow (right plot) of a Hermitian matrix diag(0, 1, 3, 5). (*b*) Complex shadow (left plot) and real shadow (right plot) of a unitary matrix diag($e^{i\frac{\pi}{8}}$, $e^{i\frac{3\pi}{8}}$, $e^{i\frac{7\pi}{8}}$, $e^{i\frac{11\pi}{8}}$).

for $0 < t < 1$. In particular, $g_3(0) = +\infty$. In [36] the case $N = 3$ is treated in terms of hypergeometric functions and we can compute

$$g_3(t) = \frac{1}{2\sqrt{2t}}\, {}_2F_1\left(\frac{1}{2}, \frac{1}{2}; 1, \frac{t-1}{2t}\right) \tag{13}$$

for $t \in (0, 1)$.

For a general $M \in M_N(\mathbb{C})$, one may write $M = A + iB$ with $A, B \in M_N(\mathbb{R})$, and by diagonalizing $(A + A^T)/2$ and $(B + B^T)/2$ we may understand the distributions of (Ax, x) and (Bx, x) separately, using the techniques above. Usually the *joint* distribution will be obscure, but we may have some hope of understanding it in certain cases. If, for example, M is normal and presented in a diagonal form, it may be possible to see how the horizontal and vertical distributions knit together.

Figure 3 shows various shadows of M when M is a 4×4 unitary (in the diagonal form). The sort of 1D shadow density seen in the left panel of figure 3(*a*) seems typical; notably, the real density of a 4×4 Hermitian is constant between the two middle eigenvalues. Presumably, the vertical density has a similar form. Figure 4 presents two examples of real shadow of generic unitary matrices of dimension 5. Support of the shadow does not coincide with a numerical range of those matrices because a generic unitary matrix cannot be diagonalized using only orthogonal matrices.

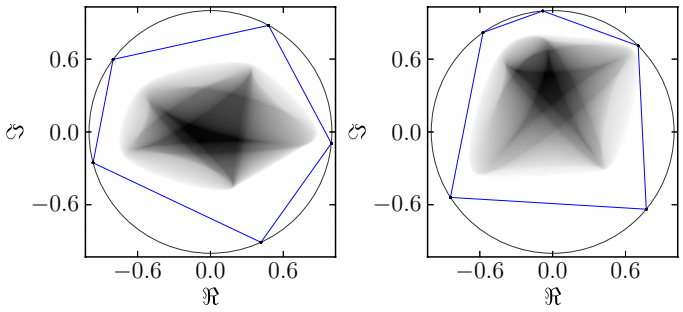

Figure 4. Real shadow of two generic unitary matrices of dimension 5 is supported on the subset of the numerical range formed by the pentagon plotted.

3.3. Real shadows and their moments

Since methods based on moments of the shadow distribution were so effective in the complex case, we may try to mimic them for the real shadow. It is not hard to adapt the method outlined at the beginning of the proof of proposition 5.1 from [26] to show that, for $\alpha \in \mathbb{N}_0^N$

$$R(\alpha) = \int_{S^{N-1}} x^\alpha = 0$$

unless each component of α is even, and that

$$R(2\beta) = \frac{\prod_{k=1}^N (\frac{1}{2})_{\beta_k}}{(\frac{N}{2})_{|\beta|}}. \tag{14}$$

Here we use the shifted factorial notation: $(x)_n = x(x+1)\dots(x+n-1)$, with the convention $(x)_0 = 1$; also $|\beta|$ denotes $\sum_1^N \beta_k$.

In principle, we can use equation (14) to evaluate the moments of the real shadow density $g(t)$ of $\mathrm{diag}(a_1, \dots, a_N)$

$$\int t^n g(t)\,\mathrm{d}t = \int_{S^{N-1}} \left(\sum_k a_k x_k^2\right)^n = \sum_{|\beta|=n} \binom{n}{\beta} a^\beta R(2\beta). \tag{15}$$

In the complex case we were able to progress beyond this point, obtaining such effective relations for the moments as the *determinant relation* (see [26, equation (10)]).

As a test case, we may try to use equation (15) to find the moments of $g_3(t)$, the real shadow density of $\mathrm{diag}(1, 0, -1)$, discussed in the previous example. We have

$$\int_{-1}^1 t^n g_3(t)\mathrm{d}t = \int_{S^2} (x_1^2 - x_3^2)^n = \sum_{k=0}^n \binom{n}{k} (-1)^k R(2(n-k), 0, 2k)$$

and finally we obtain that

$$\int_{-1}^1 t^n g_3(t)\,\mathrm{d}t = \sum_0^n \binom{n}{k} (-1)^k \frac{(\frac{1}{2})_{n-k}(\frac{1}{2})_k}{(\frac{3}{2})_n}. \tag{16}$$

It can be shown, that for even $n = 2m$ we have

$$\int_{-1}^1 t^n g_3(t)\,\mathrm{d}t = \frac{(2m+2)(2m+4)\dots(4m)}{(2m+1)(2m+3)\dots(4m+1)}.$$

To see this we start with equation (16). Changing the index of summation from k to $n-k$ shows that the sum equals $(-1)^n$ times itself, hence equals zero for odd n. Now suppose that $n = 2m$, $m = 0, 1, 2, \ldots$. The sum can be written in a hypergeometric form:

$$\int_{-1}^{1} t^n g_3(t)\,\mathrm{d}t = \frac{\left(\frac{1}{2}\right)_{2m}}{\left(\frac{3}{2}\right)_{2m}} \sum_{k=0}^{2m} \frac{(-2m)_k \left(\frac{1}{2}\right)_k}{k!\left(\frac{1}{2}-2m\right)_k}(-1)^k$$
$$= \frac{\left(\frac{1}{2}\right)_{2m}}{\left(\frac{3}{2}\right)_{2m}} {}_2F_1\left(-2m, \frac{1}{2}; 1-2m-\frac{1}{2}; -1\right).$$

Kummer's summation formula (see [38, p 10]) implies (later we set $a = -2m$, $b = \frac{1}{2}$)

$${}_2F_1(a, b; 1+a-b; -1) = 2^{-a}\,{}_2F_1\left(\frac{a}{2}, \frac{a+1}{2} - b; 1+a-b; 1\right).$$

Now we set $a = -2m$ and use the terminating form of Gauss's sum (the Chu–Vandermonde formula) to obtain

$${}_2F_1(-2m, b; 1-2m-b; -1) = 2^{2m}\,{}_2F_1\left(-m, -m+\frac{1}{2} - b; 1-2m-b; 1\right)$$
$$= 2^{2m}\frac{\left(\frac{1}{2}-m\right)_m}{(1-2m-b)_m} = 2^{2m}\frac{\left(\frac{1}{2}\right)_m}{(b+m)_m}.$$

Thus, setting $b = \frac{1}{2}$ we obtain that the integral equals

$$\int_{-1}^{1} t^n g_3(t)\,\mathrm{d}t = \frac{\frac{1}{2}}{\frac{1}{2}+2m} 2^{2m} \frac{\left(\frac{1}{2}\right)_m}{\left(\frac{1}{2}+m\right)_m}$$
$$= 2^m \frac{(2m)!}{m!\,(2m+1)\,(2m+3)\ldots(4m+1)}.$$

We use the variance of a complex random variable to give quantitative insight into figures 2–4. The calculations leading to the following formulae are based on the values of integrals of monomials over the real or complex unit spheres. Suppose A is a normal matrix, written in the form $A = VDV^\dagger$, where V is unitary and D is diagonal with entries $\lambda_1, \lambda_2, \ldots, \lambda_N$. Thus the columns of V are eigenvectors of A. Let X denote the random variable $\langle\psi|A|\psi\rangle$ and $m = \frac{1}{N}\mathrm{tr}A = \frac{1}{N}\sum_{j=1}^{N}\lambda_j$. If ψ is a random vector in the unit sphere in $\mathbb{R}^N$ or $\mathbb{C}^N$, then $\mathcal{E}X = m$ (where $\mathcal{E}$ denotes the expectation). Denote the *complex variance* $v(X) = \mathcal{E}(|X-m|^2)$, a measure of (two-dimensional) spread of X. For the complex shadow one finds

$$v(X) = \frac{1}{N(N+1)}\sum_{j=1}^{N}|\lambda_j - m|^2.$$

For the real shadow and when A can be diagonalized by a real orthogonal matrix, that is, V is orthogonal ($VV^T = I$), then

$$v(X) = \frac{2}{N(N+2)}\sum_{j=1}^{N}|\lambda_j - m|^2,$$

which is larger than the variance of the complex shadow (see figure 3(*b*)). In the general real case V is not orthogonal, then set $C(V)_{ij} = \left|\sum_{k=1}^{N} V_{ki}V_{kj}\right|^2$ for $1 \leqslant i, j \leqslant N$. Thus $C(V)$ is a symmetric unistochastic matrix, and its eigenvalues all lie in $[-1, 1]$. By straightforward computations we find

$$v(X) = \frac{1}{N(N+2)}\sum_{i,j=1}^{N}(\lambda_i - m)\overline{(\lambda_j - m)}(\delta_{ij} + C(V)_{ij}),$$

a positive quadratic form in $(\lambda_i - m)_{i=1}^N$. The eigenvalues of $I + C(V)$ lie in $[0, 2]$, and all equal 2 when V is real orthogonal.

As an example, consider the unitary Fourier matrix whose entries are primitive Nth roots of unity: $V_{jk} = \frac{1}{\sqrt{N}} \exp\left(\frac{2\pi \mathrm{i}}{N}(j-1)(k-1)\right), 1 \leqslant j, k \leqslant N$. Then $C(V)_{jk} = 1$ if $j+k \equiv 2 \bmod N$; otherwise, $C(V)_{jk} = 0$. The eigenvalues of $I+C(V)$ are 2 with multiplicity $\left\lfloor \frac{N}{2} \right\rfloor + 1$ and 0 with multiplicity $\left\lfloor \frac{N-1}{2} \right\rfloor$. The matrix $C(V)$ also contains information about approximating the eigenvectors of A by points on S^{N-1}: indeed $\min\left\{ \sum_{j=1}^N |\psi_j - cV_{jk}|^2 : |c| = 1, \psi \in S^{N-1} \right\} = 2 - \sqrt{2(1 + C(V)_{kk}^{1/2})}$. In particular if some λ_k is an extreme point in the convex hull of $\{\lambda_j : 1 \leqslant j \leqslant N\}$, then λ_k is in the real numerical range of A if and only if $\left|\sum_{j=1}^N V_{jk}^2\right| = 1$. This is illustrated by figure 4, as the real numerical range generically avoids the spectrum.

4. Product numerical shadow

Consider the shadow restricted to the set of pure product states. More formally, we assume that $\mathcal{H}_D = \mathcal{H}_N \otimes \mathcal{H}_M$, apply the definition (4) and take $\mathcal{R} = \{|\psi_A\rangle \otimes |\psi_B\rangle\}$, where $|\psi_A\rangle \in \mathcal{H}_N$, while $|\psi_B\rangle \in \mathcal{H}_M$ and these states are normalized. The set $\mathcal{R}$ of separable (product) pure states has the structure of the Cartesian product $\mathcal{R} = \mathbb{C}\mathbf{P}^{N-1} \times \mathbb{C}\mathbf{P}^{M-1} \subset \mathbb{C}\mathbf{P}^{MN-1}$.

The simplest case of $N = M = 2$ corresponds to the two-qubit case. The set of separable (product) pure states has then a form of the Cartesian product of two spheres $\mathcal{S} = \mathbf{S}^2 \times \mathbf{S}^2$. In other words this set forms a *Segre embedding*, $\mathbb{C}\mathbf{P}^1 \times \mathbb{C}\mathbf{P}^1 \subset \mathbb{C}\mathbf{P}^3$.

One may also consider the shadow with respect to real separable states. In the two-qubit case this shadow corresponds to a projection of the product of real projective spaces $\mathbb{R}\mathbf{P}^1 \times \mathbb{R}\mathbf{P}^1 \subset \mathbb{R}\mathbf{P}^3$, which forms a torus $\mathbf{S}^1 \times \mathbf{S}^1 = T^2$. Such a structure can be recognized on some plots shown in figures 5(*d*)–(*f*).

The matrices used to obtain projections are as follows:

$$B_{4a} = \begin{bmatrix} 1 & 0 & 1 & 0 \\ 0 & \mathrm{i} & 0 & 1 \\ 0 & 0 & -1 & 0 \\ 0 & 0 & 0 & -\mathrm{i} \end{bmatrix}, \quad B_{4b} = \begin{bmatrix} 1 & 0 & 0 & 1 \\ 0 & \mathrm{i} & 0 & 0 \\ 0 & 0 & -1 & 0 \\ 0 & 0 & 0 & -\mathrm{i} \end{bmatrix}, \quad B_{4c} = \begin{bmatrix} 1 & 0 & 0 & 0 \\ 0 & \mathrm{i} & 0 & 1 \\ 0 & 0 & -1 & 0 \\ 0 & 0 & 0 & -\mathrm{i} \end{bmatrix}$$

$$B_{4d} = \begin{bmatrix} 1 & 0 & 0 & 1 \\ 0 & \mathrm{i} & 1 & 0 \\ 0 & 0 & -1 & 0 \\ 0 & 0 & 0 & -\mathrm{i} \end{bmatrix}, \quad B_{4e} = \begin{bmatrix} 1 & 1 & 1 & 1 \\ 0 & \mathrm{i} & 1 & 1 \\ 0 & 0 & -1 & 1 \\ 0 & 0 & 0 & -\mathrm{i} \end{bmatrix}, \quad B_{4f} = \begin{bmatrix} \mathrm{i} & \frac{1}{2} \\ 0 & \frac{1}{2}\mathrm{i} \end{bmatrix} \otimes \mathbb{1} + \mathbb{1} \otimes \begin{bmatrix} 0 & 2 \\ 1 & \mathrm{i} \end{bmatrix}.$$

One can note that the numerical ranges presented in figure 5 have a particular structure. Matrix B_{4a} is permutation equivalent to a simple sum of two matrices, so its numerical range forms a convex hull of two ellipses: one with focal points $\{1, -1\}$ and the other $\{\mathrm{i}, -\mathrm{i}\}$. As these ellipses do intersect, their convex hull contains four interval segments. A similar situation occurs for the matrix B_{4d} where two ellipses—one with focal points $\{1, -\mathrm{i}\}$ and the other $\{\mathrm{i}, -1\}$—do not intersect and the convex hull has only two flat lines. For the matrix B_{4b} the numerical range is a convex hull of an ellipse with focal points at eigenvalues $\{1, -\mathrm{i}\}$ and the line segment between two eigenvalues $\{\mathrm{i}, -1\}$. A similar situation arises for the matrix B_{4c}.

Consider a particular case of an operator X with the tensor product structure, $X = A \otimes B$. Then its product numerical range is equal to the Minkowski product of numerical ranges $\Lambda^{\otimes}(A \otimes B) = \Lambda(A) \boxtimes \Lambda(B)$—for more information, see [21].

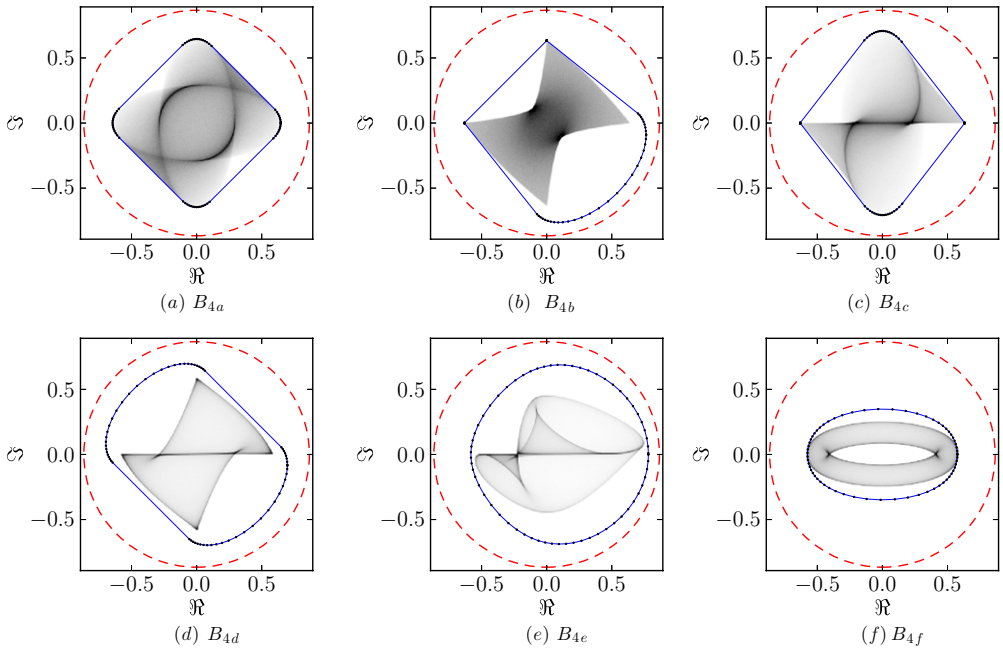

Figure 5. Product numerical shadow for illustrative operators of size $N = 4$ with respect to complex separable states; panels (*a*)–(*c*) form projections of $\mathbb{C}\mathbf{P}^1 \times \mathbb{C}\mathbf{P}^1 \subset \mathbb{C}\mathbf{P}^3$, while projections with respect to real separable states shown in panels (*d*)–(*f*) present projections of $\mathbb{R}\mathbf{P}^1 \times \mathbb{R}\mathbf{P}^1$ equivalent to the torus T^2. The dashed circle represents the image of the outsphere, while the dotted line denotes the standard numerical range. Plots are drawn for matrices translated in such a way that their traces are equal to zero and suitably rescaled as described in [28]. (*a*) B_{4a}, (*b*) B_{4b}, (*c*) B_{4c}, (*d*) B_{4d}, (*e*) B_{4e} and (*f*) B_{4f}.

In this case the shadow of $A \otimes B$ restricted to product states can be expressed by the numerical shadows of both operators

$$\mu^{\otimes}_{A\otimes B}(E) = \int_{\mathbb{C}\setminus\{0\}} \mu_B\left(\frac{E}{t}\right) \mathrm{d}\mu_A(t) + 1_{\{0\in E\}}\mu_A(\{0\}). \tag{17}$$

Here μ_A and μ_B denote the probability measures related to the numerical shadows of A and B, respectively, while $E \subset \mathbb{C}$ is a measurable subset of the complex plane.

4.1. Mean and variance for the separable numerical shadow

In the case of separable shadow of matrix $X \in \mathcal{M}_{N^2}$ it is possible to obtain explicit expressions for the mean and the variance. We have

$$\mathbb{E}(z) = \frac{1}{N^2}\,\mathrm{tr}X, \tag{18}$$

and

$$\mathbb{E}\left(z\bar{z}\right) = \frac{1}{N^2(N+1)^2}\left(|\mathrm{tr}X|^2 + \|\mathrm{tr}_A X\|^2_{\mathrm{HS}} + \|\mathrm{tr}_B X\|^2_{\mathrm{HS}} + \|X\|^2_{\mathrm{HS}}\right). \tag{19}$$

Formulae involve the partial traces $\mathrm{tr}_A X$ and $\mathrm{tr}_B X$, and follow from a more general fact given in appendix B. These expressions imply directly the following result.

$$\mathrm{Var}(z) = \frac{1}{N^2(N+1)^2}\left(-\frac{2N+1}{N^2}|\mathrm{tr}X|^2 + \|\mathrm{tr}_A X\|^2_{\mathrm{HS}} + \|\mathrm{tr}_B X\|^2_{\mathrm{HS}} + \|X\|^2_{\mathrm{HS}}\right). \tag{20}$$

4.2. Separable numerical shadow for a diagonal matrix

Consider a diagonal matrix X defined on a composite Hilbert space, $\mathcal{H}_D = \mathcal{H}_N \otimes \mathcal{H}_M$ of dimension $D = NM$. Its diagonal elements forming the spectrum $\{x_i\}_{i=1}^D$ can be also represented by two indices: $\{y_{\mu\nu}\}$ with $\mu = 1, \ldots, N$ and $\nu = 1, \ldots, M$.

Let $|1, 1\rangle$ be an arbitrary fixed pure product state in $\mathcal{H}_D$, so the set of random separable pure states can be obtained as $|\psi\rangle = U|1, 1\rangle = W \otimes V|1, 1\rangle$, where $W \in \mathrm{U}(N)$ and $V \in \mathrm{U}(M)$ are independent random unitary matrices distributed according to the Haar measure. Thus the expansion coefficients of the product state $|\psi\rangle$ read $(U_{11}, U_{12}, \ldots, U_{1D}) = (W_{11}V_{11}, \ldots, W_{1N}V_{1M})$.

The *separable numerical shadow* of the diagonal operator X is defined as the density distribution of random numbers $z := \langle\psi|X|\psi\rangle$, where $|\psi\rangle$ is a separable random state defined by random unitaries U and V. In this case one has

$$z := \langle 1, 1|(W^\dagger \otimes V^\dagger)X(W \otimes V)|1, 1\rangle = \sum_{i=1}^{D} x_i |U_{1i}|^2 = \sum_{\mu=1}^{N}\sum_{\nu=1}^{M} y_{\mu\nu}|W_{1\mu}|^2|V_{1\nu}|^2 = x \cdot r, \quad (21)$$

where r is a real probability vector of size $D = NM$. It can be considered as a tensor product of two probability vectors $p \in \Delta_{N-1}$ and $q \in \Delta_{M-1}$, since its components read $r_{\mu\nu} = p_\mu q_\nu$ with $\mu = 1, \ldots N$ and $\nu = 1, \ldots, M$.

Thus the separable numerical shadow of a diagonal operator can be considered as a projection of the *Cartesian product* of classical probability simplices, $\Delta_{N-1} \times \Delta_{M-1}$. In the simplest case of $D = 4 = 2 \times 2$, the Cartesian product of two intervals (1-simplices) forms a square, which lives inside the tetrahedron of the four-dimensional probability vectors. As in the previous case we can distinguish two probability measures in the space of unitary matrices. They lead to

(C) *Complex separable shadow*, generated by the Haar measure on $\mathrm{U}(N)$ and $\mathrm{U}(M)$, for which both probability vectors p and q are distributed uniformly with respect to the Lebesgue measure on the simplices Δ_{N-1} and Δ_{M-1}, respectively.

(D) *Real separable shadow*, generated by the Haar measure on the orthogonal groups $\mathrm{O}(N)$ and $\mathrm{O}(M)$, which lead to the statistical measure (Dirichlet measure with $s = 1/2$) in both simplices.

Note that in this case the separable shadow of X is supported on its *product numerical range* [21], which in general forms a proper subset of the convex hull of the spectrum. The product structure of the classical probability vector r in (21), generalized for a multiple tensor product structure, is consistent with the parametrization of the product numerical range described in [21, proposition 12].

5. Maximally entangled numerical shadow

Consider an operator X acting on a Hilbert space with a tensor product structure, $\mathcal{H} = \mathcal{H}_A \otimes \mathcal{H}_B$. For simplicity let us assume that the dimensions of both subspaces are equal to N, so the total dimension reads $D = N^2$. Among all pure states of the $N \times N$ system, one distinguishes the set $\mathcal{E}$ of maximally entangled states. It contains the states equivalent with respect to a local unitary operation $U_A \otimes U_B$ to the generalized Bell state, $|\psi_+\rangle = \frac{1}{\sqrt{N}} \sum_i |i, i\rangle$. Thus the set of maximally entangled states has the structure of $\mathrm{U}(N)/\mathrm{U}(1) = \mathrm{SU}(N)/Z_N$, where Z_N is the discrete permutation group [13], [8, chapter 15]. Choosing $\mathcal{E}$ for the set R in (4) we define the shadow $P_X^{\mathcal{E}}(z)$ of an operator X with respect to the maximally entangled states. The corresponding probability measure will be denoted as $d\mu_X^{\mathcal{E}}(z)$.

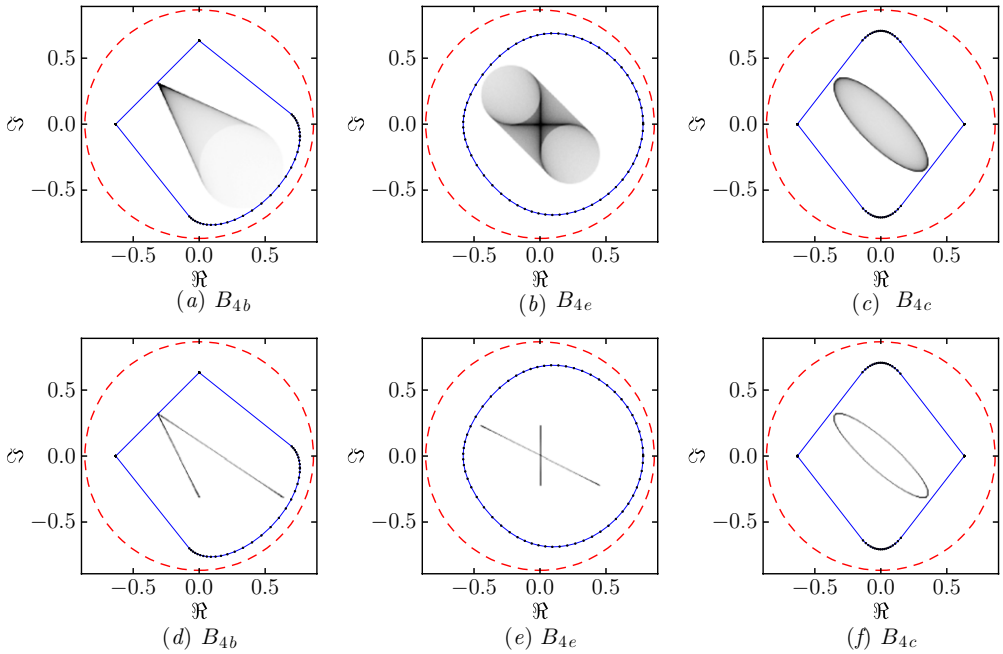

Figure 6. Entangled numerical shadow for illustrative operators of size $N = 4$ with respect to complex maximally entangled states; panels (*a*)–(*c*) form projections of $\mathrm{U}(2)/\mathrm{U}(1) \sim \mathbb{R}\mathbf{P}^3$, while projections with respect to real entangled states shown in panels (*d*)–(*f*) present projections of $\mathrm{O}(2)/\mathrm{U}(1)$ equivalent to a circle $\mathbf{S}^1$. Plots are drawn for matrices translated in such a way that their traces are equal to zero and suitably rescaled as described in [28]. (*a*) B_{4b}, (*b*) B_{4e}, (*c*) B_{4c}, (*d*) B_{4b}, (*e*) B_{4e} and (*f*) B_{4c}.

5.1. Two-qubit case: $D = 2 \times 2$

In the simplest case of 2×2 Hilbert space, the set $\mathcal{E}$ of maximally entangled states has the structure $\mathrm{U}(2)/\mathrm{U}(1) = \mathbb{R}\mathbf{P}^3$—see [8]. Hence the numerical shadow of an operator A of order 4 with respect to the complex maximally entangled states can be considered as a projection of the real projective space on the plane—see the shadow for some illustrative operators presented in figures 6(*a*)–(*c*).

If one considers a further restriction and studies the shadow with respect to *real* maximally entangled states, the result can be interpreted as an image of the space $\mathrm{O}(2)/\mathrm{O}(1) = \mathbb{R}\mathbf{P}^1 = \mathbf{S}^1$. Observe that the illustrative shadows obtained in this case and presented in figures 6(*d*)–(*f*) show indeed projections of a circle onto the complex plane.

In the special case of a diagonal operator B of size 4, its shadow with respect to complex maximally entangled states can be identified with a standard shadow of a reduced operator B' of size 2. This fact is formulated in the following proposition, proved in appendix A.

Proposition 3. *Consider a diagonal matrix of order 4, $X = \mathrm{diag}(d_1, d_2, d_3, d_4)$ which acts on a composite Hilbert space $\mathcal{H} = \mathcal{H}_A \otimes \mathcal{H}_B$ and the reduced matrix $Y = Y(X) = \frac{1}{2}\mathrm{diag}(d_1 + d_4, d_2 + d_3)$. Then the numerical shadow $P_X^{\mathcal{E}}(z)$ of X with respect to complex maximally entangled states $\mathcal{E}$ is equal to the standard numerical shadow $P_Y(z)$ of the reduced matrix $Y(X)$ of order 2.*

5.2. Two-qubit case: $D = N \times N$

In this general case the set $\mathcal{E}$ of maximally entangled states forms a manifold of $(N^2 - 1)$ real dimensions with the structure of $\mathrm{U}(N)/\mathrm{U}(1)$ [8]. In the case of the shadow with respect to real maximally entangled states, the space under consideration reads $\mathrm{O}(N)/\mathrm{O}(1)$.

To analyse the entangled shadow of a diagonal matrix, we can perform initial steps used to prove proposition 3. It will be convenient to use a slightly different notation and consider a diagonal matrix X of size $D = N^2$ acting on a tensor product space $\mathcal{H} = \mathcal{H}_A \otimes \mathcal{H}_B$ with entries $X_{(i,j),(i,j)}$ where $i, j = 1, \ldots, N$. Consider a local unitary matrix $U^{(A)} \otimes U^{(B)}$ where $U^{(A)}, U^{(B)} \in \mathrm{U}(N)$. The entangled unit state v has entries

$$v_{(i,j)} = \frac{1}{\sqrt{N}} \sum_{k=1}^{N} U^{(A)}_{ik} U^{(B)}_{jk} = \frac{1}{\sqrt{N}} U_{ij}, \tag{22}$$

where $U = U^{(A)}(U^{(B)})^T$. For purposes of numerical shadow the integration with respect to the Haar measure over both matrices $U^{(A)}$ and $U^{(B)}$ can be replaced by a single integration over the N-dimensional random unitary matrix U. Observe $U \mapsto \overline{U}$ is a real automorphism of $\mathrm{U}(N)$ invariant for the Haar measure.

Taking a diagonal matrix $X_{(i_1,j_1),(i_2,j_2)} = \delta(i_1, i_2)\,\delta(j_1, j_2)\,C_{i_1,j_1}$, we find its expectation value for a random pure state v

$$v^\dagger A v = \frac{1}{N} \sum_{i,j=1}^{N} C_{ij} \left|U_{ij}\right|^2 = \frac{1}{N} \mathrm{tr}\left(CB^T\right).$$

Here we reshape the diagonal matrix X of order N^2 to obtain a matrix C of order N with entries C_{ij}, while B stands for a unistochastic matrix, $B_{ij} := |U_{ij}|^2$, for $i, j = 1, \ldots, N$. The case $N = 2$ studied above relied on the simple nature of the set of unistochastic matrices of order 2, equivalent to an interval. It is known that the structure of unistochastic matrices for $N \geqslant 3$ is complicated and interesting [32, 33]. Thus we are not able to formulate a direct generalization of proposition 3 for the $N \times N$ problem.

For the case of 3×3 matrices, consider the function

$$v^\dagger A v = \tfrac{1}{3}\mathrm{tr}(CB^T),$$

where the (variable) unistochastic matrix reads

$$B = \begin{bmatrix} b_1 & b_2 & 1 - b_1 - b_2 \\ b_3 & b_4 & 1 - b_3 - b_4 \\ 1 - b_1 - b_3 & 1 - b_2 - b_4 & b_1 + b_2 + b_3 + b_4 - 1 \end{bmatrix}.$$

Given the matrix C, let $C_{i\cdot} = \sum_{k=1}^{3} C_{ik}$, $C_{\cdot j} = \sum_{k=1}^{3} C_{kj}$, for $1 \leqslant i, j \leqslant 3$, and $C_{\cdot\cdot} = \sum_{i,j=1}^{3} C_{ij}$. For simplification we set

$$\gamma_{ij} = C_{ij} - \tfrac{1}{3}C_{i\cdot} - \tfrac{1}{3}C_{\cdot j} + \tfrac{1}{9}C_{\cdot\cdot}.$$

One can observe that the row and column sums of $[\gamma_{ij}]$ are zero and

$$v^\dagger A v = \frac{1}{3}\mathrm{tr}\begin{bmatrix} 4b_1 + 2b_2 + 2b_3 + b_4 - 3 & 2b_1 + 4b_2 + b_3 + 2b_4 - 3 \\ 2b_1 + b_2 + 4b_3 + 2b_4 - 3 & b_1 + 2b_2 + 2b_3 + 4b_4 - 3 \end{bmatrix} \begin{bmatrix} \gamma_{11} & \gamma_{12} \\ \gamma_{21} & \gamma_{22} \end{bmatrix} + \frac{1}{9}C_{\cdot\cdot}.$$

Without loss of generality we can assume $C_{\cdot\cdot} = 0$. Powers of $v^\dagger A v$ can be integrated using the formula from [39, proposition 3.3]:

$$\int_{\mathrm{U}(3)} b_1^{n_1} b_2^{n_2} b_3^{n_3} b_4^{n_4} \mathrm{d}m = \frac{n_1! n_2! n_3! n_4!\,(2)_{n_2+n_3}\,(2)_{n_1+n_2+n_4}}{(3)_{n_1+n_2+n_3+n_4}\,(2)_{n_2+n_4}\,(2)_{n_1+n_2}\,(2)_{n_3}} \times {}_4F_3\left(\begin{matrix} -n_1, -n_2, -n_4, 1 + n_3 \\ 1, 2 + n_3, -1 - n_1 - n_2 - n_4 \end{matrix}; 1\right),$$

where dm denotes the Haar measure on U(3).

For example,

$$\int_{\mathrm{U}(3)} \left(v^{\dagger}Av\right)^2 \mathrm{d}m = \frac{1}{72}\left\{3\sum_{i,j=1}^{2}\gamma_{ij}^2 + \left(\sum_{i,j=1}^{2}\gamma_{ij}\right)^2 + 2\left(\gamma_{11}+\gamma_{22}\right)\left(\gamma_{12}+\gamma_{21}\right)\right\}.$$

There is an interesting special case when one of the variables b_i, say b_4, does not appear in $v^{\dagger}Av$. The triple (b_1, b_2, b_3) is a point in the pyramid with square base $\{(0, b_2, b_3) : 0 \leqslant b_2, b_3 \leqslant 1\}$ and vertex $(1, 0, 0)$. The induced measure (from U (3)) on the pyramid is $\frac{2}{1-b_1}\,\mathrm{d}b_1\,\mathrm{d}b_2\,\mathrm{d}b_3$. The numerical range of A is an affine image of the pyramid; hence it is the convex hull of the images of the vertices of the pyramid, $\{(1, 0, 0)\,, (0, 1, 0)\,, (0, 0, 1)\,, (0, 1, 1)\,, (0, 0, 0)\}$, that is, a convex polygon. For three arbitrary complex numbers z_1, z_2, z_3, let

$$\begin{bmatrix}\gamma_{11} & \gamma_{12}\\ \gamma_{21} & \gamma_{22}\end{bmatrix} = \begin{bmatrix}-6z_1 - 6z_2 & 3z_1 + 3z_3\\ 3z_2 + 3z_3 & -3z_3\end{bmatrix},$$

then $v^{\dagger}Av = (z_3 - 2z_1 - 2z_2)\,b_1 + (z_3 - z_1)\,b_2 + (z_3 - z_2)\,b_3 + z_1 + z_2 - z_3$. The vertices of the pyramid are mapped to $\{z_1, z_2, z_3, -z_1 - z_2, z_1 + z_2 - z_3\}$. It is possible that these points form a (not regular) pentagon. For example let $z_1 = 1$, $z_2 = \mathrm{i}$, $z_3 = -\frac{3}{4} + \frac{\mathrm{i}}{8}$, then the range is the convex hull of $\left\{1, \frac{7}{4} + \frac{7}{8}\mathrm{i}, \mathrm{i}, -\frac{3}{4} + \frac{\mathrm{i}}{8}, -1 - \mathrm{i}\right\}$.

It may not be easy to find the shadow measure explicitly, but one expects a higher density in the neighbourhood of $-z_1 - z_2$, the image of $b = (1, 0, 0)$. Fix $\varepsilon > 0$ and consider the set $B_\varepsilon = \{(b_1, b_2, b_3) : 1 - \varepsilon < b_1 < 1, 0 < b_2, b_3 < 1 - b_1\}$. The normalized volume of B_ε is ε^3 and the U (3) measure of B_ε is ε^2, so the relative density is $\frac{1}{\varepsilon}$.

5.3. Mean and variance for the entangled shadow

It is possible to obtain explicit expressions for the mean and the variance of the entangled shadow $\mathrm{d}\mu_X^{\mathcal{E}}$ of matrix X acting on the $N \times N$ Hilbert space $\mathcal{H} = \mathcal{H}_A \otimes \mathcal{H}_B$. The following results

$$\mathbb{E}\,(z) = \int_{\mathbb{C}} z\,\mathrm{d}\mu_X^{\mathcal{E}}\,(z) = \frac{1}{N^2}\mathrm{tr}X, \tag{23}$$

and

$$\begin{aligned}\mathbb{E}\,(z\bar{z}) = \int_{\mathbb{C}} z\bar{z}\,\mathrm{d}\mu_X^{\mathcal{E}}\,(z) &= \frac{1}{N^2\left(N^2-1\right)}\left\{\|X\|_{\mathrm{HS}}^2 + |\mathrm{tr}X|^2\right\}\\ &\quad - \frac{1}{N^3\left(N^2-1\right)}\left\{\|\mathrm{tr}_A X\|_{\mathrm{HS}}^2 + \|\mathrm{tr}_B X\|_{\mathrm{HS}}^2\right\},\end{aligned} \tag{24}$$

which involve the partial traces $\mathrm{tr}_A X$ and $\mathrm{tr}_B X$, are derived in appendix B from a more general fact. These expressions imply directly the following result.

Proposition 4. *The expected squared distance from the mean with respect to the entangled shadow* $\mathrm{d}\mu_X^{\mathcal{E}}$ *reads*

$$\begin{aligned}\int_{\mathbb{C}} |z - \mathbb{E}\,(z)|^2\,\mathrm{d}\mu_X^{\mathcal{E}}\,(z) &= \frac{1}{N^2\left(N^2-1\right)}\left\{\|X\|_{\mathrm{HS}}^2 + \frac{1}{N^2}|\mathrm{tr}X|^2\right\}\\ &\quad - \frac{1}{N^3\left(N^2-1\right)}\left\{\|\mathrm{tr}_A X\|_{\mathrm{HS}}^2 + \|\mathrm{tr}_B X\|_{\mathrm{HS}}^2\right\}.\end{aligned} \tag{25}$$

Let us apply these formulae in the special case of a diagonal matrix $X_{(i_1,j_1),(i_2,j_2)} = \delta(i_1,i_2)\,\delta(j_1,j_2)\,C_{i_1,j_1}$. In this case the necessary ingredients of (25) simplify considerably, e.g.

$$\mathrm{tr}X = \sum_{i,j=1}^{N} C_{ij}, \qquad \mathrm{tr}\left(XX^{\dagger}\right) = \sum_{i,j=1}^{N} \left|C_{ij}\right|^2,$$

$$\left(\mathrm{tr}_A X\right)_{j_1,j_2} = \delta(j_1,j_2) \sum_{i=1}^{N} C_{i,j_1}, \qquad \left(\mathrm{tr}_B X\right)_{i_1,i_2} = \delta(i_1,i_2) \sum_{j=1}^{N} C_{i_1,j},$$

$$\mathrm{tr}\left(\left(\mathrm{tr}_A X\right)\left(\mathrm{tr}_A X^{\dagger}\right)\right) = \sum_{j=1}^{N} \left|\sum_{i=1}^{N} C_{ij}\right|^2, \qquad \mathrm{tr}\left(\left(\mathrm{tr}_B X\right)\left(\mathrm{tr}_B X^{\dagger}\right)\right) = \sum_{i=1}^{N} \left|\sum_{j=1}^{N} C_{ij}\right|^2.$$

For the easy case $N = 2$ we find $\mathbb{E}(|z - \mathbb{E}(z)|^2) = \frac{1}{48}|C_{11} + C_{22} - C_{12} - C_{21}|^2$, in agreement with the previous calculations.

6. Shadow and dynamics of quantum entanglement

In previous sections we analysed the entire set of quantum states with its subsets and their projections onto a plane. In this section we specify a concrete quantum dynamics (in general non-unitary), choose an initial quantum state $\rho(0)$ and following [28] we analyse its trajectory projected on the plane of a shadow of a selected non-Hermitian operator A. In particular we will be interested in dynamics of quantum entanglement, so the separable shadow of A will be used as a background for the trajectory obtained from the expectation values, $z(t) = \mathrm{Tr}A\rho(t)$.

Investigation of the dynamics of quantum entanglement was initiated in [40] in which the evolution of certain measures of entanglement in time was studied for a model non-unitary dynamics of a two-qubit system and several qualitatively different scenarios of behaviour of entanglement in time were identified. In particular, revivals of entanglement in time and an effect of sudden decay of quantum entanglement were reported. The latter effect was later called *entanglement sudden death* by Yu and Eberly [41, 42] and the dynamics of entanglement was studied by several authors in various setups [43–47].

In general, all these dynamical effects can be explained in a simple geometric manner, if one takes into account the structure of the set of separable states analysed in [2]. As the convex set $\mathcal{Q}_D^{\mathrm{sep}}$ of separable mixed states of a bipartite system occupies the central part of the set $\mathcal{Q}_D$ of all states of size D, entanglement revivals occur if the unitary dynamics moves the initial state several times across the separability boundary. On the other hand, the entanglement sudden death effect takes place, if the decoherence is so strong that the initially pure state gets mixed in such a pace that it crosses the separability boundary only once. These possible scenarios are shown on a schematic sketch, used in conference talks for several years—see figure 7(*a*).

Making use of the technique of numerical shadow, we are now in a position to observe similar behaviour of entanglement for a concrete choice of quantum dynamics and initial states. Consider the following discrete-time dynamic quantum process of a system consisting of two qubits [40]. The system is assumed to be initially described by a maximally entangled pure state, $\rho_0 = \frac{1}{2}(|00\rangle + |11\rangle)(\langle 00| + \langle 11|)$. The discrete time evolution of the system is given by a one-step unitary evolution expressed by Pauli matrices, $U = \mathrm{e}^{\mathrm{i}\alpha\sigma_x\otimes\sigma_y}$, followed by

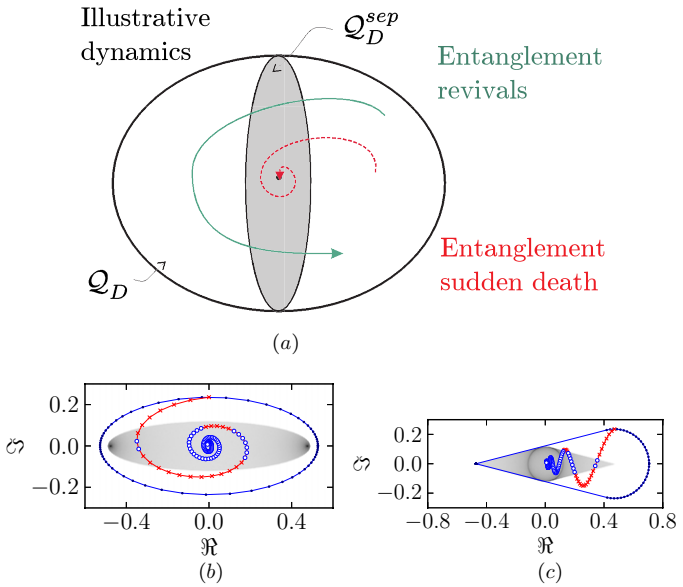

Figure 7. Dynamics of quantum entanglement. (*a*) Schematic figure often used to explain dynamics of quantum entanglement. (*b*) Actual trajectory observed with the separable shadow of an exemplary matrix X_1 in the background. All points outside this shadow are entangled (red crosses along the trajectory), while the points projected into the centre of the separable shadow are separable (blue circles along the trajectory). (*c*) The same trajectory observed by matrix X_2. States of the trajectory projected into the separable shadow are typically separable.

an action of the depolarizing channel acting locally on the second qubit,

$$\Phi(\rho) = \sqrt{(1-\beta)}\mathbb{1}_4\,\rho\,\sqrt{(1-\beta)}\mathbb{1}_4 + \sum_{p\in\{x,y,z\}} \sqrt{\frac{1}{3}\beta}\mathbb{1}_2 \otimes \sigma_p\,\rho\,\sqrt{\frac{1}{3}\beta}\mathbb{1}_2 \otimes \sigma_p, \tag{26}$$

so that $\rho_{t+1} = U\Phi(\rho_t)U^\dagger$.

As the initial state is chosen to be pure, the trajectory begins at the boundary of the set of mixed states. As time t increases the trajectory plunges into the set of mixed states periodically crossing the set of entangled states. An artist's impression of such processes is depicted in figure 7(*a*), where the outer oval corresponds to the set of the pure states, its interior corresponds to the set of all mixed states, ellipse corresponds to the set of separable states and spirals depict the trajectory.

Let us fix the parameters of the discussed process, by setting the interaction strength $\alpha = 0.1$ and decoherence rate $\beta = 0.03$. We arbitrarily chose two matrices

$$X_1 = \begin{bmatrix} -1 & 0 & 0 & \mathrm{i} \\ 0 & 1 & 0 & 0 \\ 0 & 0 & -1 & 0 \\ 0 & 0 & 0 & 1 \end{bmatrix} \text{ and } X_2 = \begin{bmatrix} 1 & 0 & 0 & \mathrm{i} \\ 0 & -1 & 0 & 0 \\ 0 & 0 & -1 & 0 \\ 0 & 0 & 0 & 1 \end{bmatrix}, \tag{27}$$

which allow us to project the trajectory ρ_t onto the complex plane. We can calculate the images of the trajectory $z_t^{(k)} = \mathrm{tr}(\rho_t^\dagger X_k)$, $k = 1, 2$ and superimpose them on the separable shadows of matrices X_k. The resulting images are shown in figure 7 (*b*) and (*c*). The red crosses indicate entangled states and blue circles indicate separable states.

It can be easily seen that by choosing an appropriate observation matrix, it is convenient to observe the dynamics of entanglement in the process. In the general case for any given

trajectory, it is hardly possible to find such an observation matrix whose product numerical range contains only images of separable states, but images of entangled states always lie outside of product numerical range. Therefore product numerical range and separable shadow of a matrix are useful tools to visualize dynamics of entanglement, the effects of entanglement sudden death and entanglement revival.

7. Multipartite systems

It is natural to ask about the properties of the numerical shadow in the case when one aims to study composite quantum systems consisting of more than two subsystems.

Let us consider the simplest case of a multipartite quantum system, i.e. a system composed of three qubits. In this case $N = 2^3 = 8$. As an example we take a unitary matrix U_8 of size 8 written in the standard computational basis $\{|0, 0, 0\rangle, |0, 0, 1\rangle, \ldots, |1, 1, 1\rangle\}$

$$U_8 = \mathrm{diag}(1, \mathrm{e}^{\frac{2\mathrm{i}\pi}{3}}, \mathrm{e}^{\frac{2\mathrm{i}\pi}{3}}, \mathrm{e}^{-\frac{2\mathrm{i}\pi}{3}}, \mathrm{e}^{\frac{2\mathrm{i}\pi}{3}}, \mathrm{e}^{-\frac{2\mathrm{i}\pi}{3}}, \mathrm{e}^{-\frac{2\mathrm{i}\pi}{3}}, 1). \tag{28}$$

The product numerical range of this operator is not simply connected [19, 21], so it is instructive to study the shadow of U_8 with respect to the space of

(a) all pure states (standard shadow);
(b) product states (product shadow), $|\psi\rangle_{\mathrm{sep}} = U_A \otimes U_B \otimes U_C|0, 0, 0\rangle$;
(c) GHZ-entangled states, $|\psi\rangle_{\mathrm{GHZ}} = U_A \otimes U_B \otimes U_C(|0, 0, 0\rangle + |1, 1, 1\rangle)/\sqrt{2}$;
(d) so-called W-entangled states, $|\psi\rangle_{\mathrm{W}} = U_A \otimes U_B \otimes U_C(|1, 0, 0\rangle + |0, 1, 0\rangle + |0, 0, 1\rangle)/\sqrt{3}$.

Here U_A, U_B, U_C are independent random unitary matrices taken from U(2) with respect to the Haar measure. Figure 8 presents the shadows generated by matrix U_8 with respect to those classes of states.

Observe that a generic operator acting on the three-qubit system leads to different shadows, if they are taken with respect to GHZ states and the W states. This is a consequence of the different topology of the orbits with respect to local unitary transformations produced by these two classes of entangled states. Study of numerical shadows restricted to certain classes of entangled states can contribute to a better understanding of the geometry of the manifold of locally equivalent states.

Investigations of the restricted shadows of operators acting on multipartite systems lead to a wide class of interesting problems which in general are difficult to solve. However, some results obtained in the previous sections for the bipartite setup can be generalized for multipartite systems.

Consider an operator acting on the composite Hilbert space describing m-partite system of dimensions $N_1, N_2, \ldots, N_m$, respectively. Its shadow with respect to separable states $|\Psi\rangle = |\psi_1\rangle \otimes |\psi_2\rangle \otimes \ldots |\psi_m\rangle$ leads to classical product measures on a simplex of a composed dimension $D = N_1 N_2 \cdots N_m - 1$, induced by the Dirichlet measures on m simplices of the dimension $(N_i - 1)$ with $i = 1, \ldots, m$.

8. Concluding remarks

In this work we propose to combine the notion of restricted numerical range with the numerical shadow of an operator which is a probability measure on the complex plane. On the one hand the numerical shadow can be investigated for a given operator X. On the other hand, one may analyse the shadows of all operators of a fixed dimension D, which can be considered as projections of the set of all pure states of size D onto a plane.

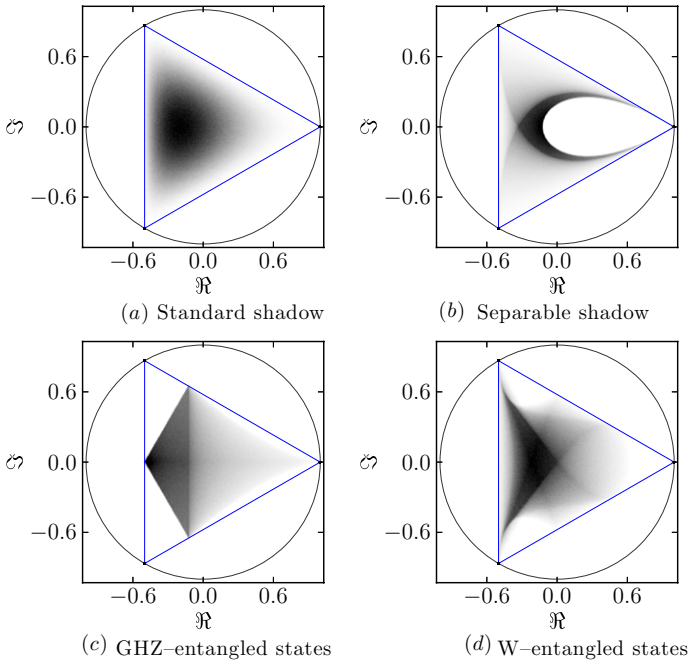

Figure 8. Restricted shadows given by the matrix from equation (28). In each case the probability distribution is supported on a subset of a numerical range, namely restricted numerical range. In the general case this subset is not convex and the restricted numerical shadow can be supported on a non-convex set. (*a*) Standard shadow. (*b*) Separable shadow. (*c*) GHZ-entangled states. (*d*) *W*-entangled states.

In a similar way it could be interesting to study the shadow of a given operator X with respect to various sets of pure states. For instance, in this work, we analysed the standard shadow with respect to complex states and the shadow restricted to real states. For operators acting on composite Hilbert spaces, one can additionally study the shadow with respect to separable or maximally entangled states, complex or real. Note that in general the restricted numerical range is not convex [24, 25], which implies that the restricted numerical shadow can be supported on non-convex sets.

Following the complementary strategy one may take the set of all operators of a given dimension and analyse their shadows restricted to a certain class of states. These probability distributions on the complex plane convey some information about the structure of these specific subsets of the set of all quantum states. Consider for instance the simplest Hilbert space with a tensor product structure $\mathcal{H}_2 \otimes \mathcal{H}_2$. Then the standard shadow carries information about the set of all pure states Ω_4 which forms the complex projective space $\mathbb{C}\mathbf{P}^3$, while the shadow restricted to real states corresponds to the real projective space $\mathbb{R}\mathbf{P}^3$.

In a similar way, the shadows of matrices of order 4 with respect to separable states illustrate the projections of the product of two spheres $\mathbb{C}\mathbf{P}^1 \times \mathbb{C}\mathbf{P}^1 = \mathbf{S}^2 \times \mathbf{S}^2$, while the real separable shadow corresponds to projections of a torus $\mathbb{R}\mathbf{P}^1 \times \mathbb{R}\mathbf{P}^1 = \mathbf{S}^1 \times \mathbf{S}^1 = T^2$. The shadow with respect to maximally entangled states (also called briefly the *entangled shadow*) represents the set $\mathcal{E} = \mathrm{U}(2)/\mathrm{U}(1)$ also equivalent to real projective space $\mathbb{R}\mathbf{P}^3$. In the case of real entangled shadow we observe projections of the set $\mathcal{E}_R = \mathrm{O}(2)/\mathrm{O}(1)$ equivalent to the circle $\mathbb{R}\mathbf{P}^1 \sim \mathbf{S}^1$.

The notion of separable shadow is useful to analyse the dynamics of quantum entanglement. For a given initial quantum state $\rho(0)$ and a certain dynamics, we select a non-Hermitian matrix A and study trajectories on the complex plane formed by the time evolution of its expectation value, $z(t) = \mathrm{Tr}A\rho(t)$. Investigations of such a trajectory superimposed on the separable shadow of A contribute to our understanding of the dynamics of quantum entanglement and allow us to visualize the effects of entanglement sudden death and entanglement revivals.

The notion of restricted numerical range is easily formulated for operators acting on the Hilbert space with the multiple tensor product structure [25], which correspond to multipartite quantum systems. Therefore it is natural to define a restricted numerical shadow for various classes of quantum states of multipartite systems. For instance, in the simplest case of a three-qubit system, described in the Hilbert space $\mathcal{H}_8 = \mathcal{H}_2^{\otimes 3}$ one may distinguish two classes of maximally entangled states called GHZ and W, which cannot be locally converted in any direction [35]. Studying numerical shadows of matrices of order 8, restricted to GHZ states or W states, we are thus in a position to investigate the differences between the structure of these two important classes of three-qubit quantum entangled states.

In conclusion, we have introduced the notion of the restricted numerical shadow of an operator and established its basic properties. On the one hand we believe that this topic is interesting from the mathematical point of view, as it relates operator theory and probability. Moreover, we are tempted to expect that further investigations of the restricted numerical shadow will contribute to a better understanding of the geometry of quantum entanglement, so that they become directly applicable to the theory of quantum information.

Acknowledgments

It is a pleasure to thank E Gutkin for fruitful discussions. Work by JAH was supported in part by an NSERC of Canada research grant. Work by PG was supported by the Polish National Science Centre under the grant number N N516 481840, ZP was supported by the Polish National Science Centre under the research project N N514 513340, JAM was supported by the Polish Ministry of Science and Higher Education under the research project IP2011 036371, while KZ acknowledges support by the Polish Ministry of Science and Higher Education grant number N202 090239. Numerical calculations presented in this work were performed on the `Leming` server of The Institute of Theoretical and Applied Informatics, Polish Academy of Sciences.

Appendix A. Proof of proposition 3

To analyse properties of the shadow with respect to complex maximally entangled states for an operator acting on the 2×2 Hilbert space, let us analyse the structure of a local unitary transformation $U^{(A)} \otimes U^{(B)}$ acting on $\mathcal{H} = \mathcal{H}_A \otimes \mathcal{H}_B$. Consider two generic elements of U (2)

$$U^{(A)} = \begin{bmatrix} \mathrm{e}^{\mathrm{i}(\psi_1+\phi_1)}\cos\theta_1 & -\mathrm{e}^{\mathrm{i}(\psi_1-\phi_2)}\sin\theta_1 \\ \mathrm{e}^{\mathrm{i}(\psi_1+\phi_2)}\sin\theta_1 & \mathrm{e}^{\mathrm{i}(\psi_1-\phi_1)}\cos\theta_1 \end{bmatrix},$$

$$U^{(B)} = \begin{bmatrix} \mathrm{e}^{\mathrm{i}(\psi_2+\phi_3)}\cos\theta_2 & -\mathrm{e}^{\mathrm{i}(\psi_2-\phi_4)}\sin\theta_2 \\ \mathrm{e}^{\mathrm{i}(\psi_2+\phi_4)}\sin\theta_2 & \mathrm{e}^{\mathrm{i}(\psi_2-\phi_3)}\cos\theta_2 \end{bmatrix},$$

where $-\pi < \phi_j \leqslant \pi, 0 \leqslant \psi_j < \pi, 0 \leqslant \theta_j \leqslant \frac{\pi}{2}$ and the Haar measure (for $U^{(A)}$) is

$$\mathrm{d}m(U) = \frac{1}{2\pi^3}\mathrm{d}\psi_1\mathrm{d}\phi_1\mathrm{d}\phi_2\sin\theta_1\cos\theta_1\mathrm{d}\theta_1.$$

Taking tensor products of corresponding columns of $U^{(A)}$ and $U^{(B)}$ and adding them, we obtain a parametrization of an entangled state

$$v = \frac{1}{\sqrt{2}} \begin{bmatrix} U_{11}^{(A)} U_{11}^{(B)} + U_{12}^{(A)} U_{12}^{(B)} \\ U_{21}^{(1)} U_{11}^{(2)} + U_{22}^{(A)} U_{12}^{(B)} \\ U_{11}^{(1)} U_{21}^{(2)} + U_{12}^{(A)} U_{22}^{(B)} \\ U_{21}^{(1)} U_{21}^{(2)} + U_{22}^{(A)} U_{22}^{(B)} \end{bmatrix}.$$

Consider a diagonal matrix of order 4, $X = \operatorname{diag}(d_1, d_2, d_3, d_4)$, so that its expectation value for a maximally entangled state reads

$v^\dagger X v = \frac{1}{2}(d_1 + d_4) q_1 + \frac{1}{2}(d_2 + d_3) q_2,$

$q_1 = \cos^2\theta_1 \cos^2\theta_2 + \sin^2\theta_1 \sin^2\theta_2 + \frac{1}{2}\sin 2\theta_1 \sin 2\theta_2 \cos(\phi_1 + \phi_2 + \phi_3 + \phi_4),$

$q_2 = \cos^2\theta_1 \sin^2\theta_2 + \sin^2\theta_1 \cos^2\theta_2 - \frac{1}{2}\sin 2\theta_1 \sin 2\theta_2 \cos(\phi_1 + \phi_2 + \phi_3 + \phi_4).$

Observe that $q_1 + q_2 = 1$. Compare this situation to the complex shadow of the reduced operator $Y = Y(X)$

$$Y = \begin{bmatrix} \frac{1}{2}(d_1 + d_4) & 0 \\ 0 & \frac{1}{2}(d_2 + d_3) \end{bmatrix},$$

$$x^\dagger Y x = \frac{1}{2}(d_1 + d_4)|x_1|^2 + \frac{1}{2}(d_2 + d_3)|x_2|^2,$$

where x belongs to the unit sphere $\mathbf{S}^1$ in $\mathbb{C}^2$. We know that

$$\int_{\mathbf{S}^1} |x_1|^{2n} |x_2|^{2k} \, \mathrm{d}\mu(x) = \frac{n!k!}{(k+n+1)!}, k, n = 0, 1, 2, \ldots.$$

To identify the two shadows it only remains to show

$$\int_{\mathrm{U}(2)\times\mathrm{U}(2)} q_1^n q_2^k \, \mathrm{d}m\left(U^{(1)}\right) \mathrm{d}m\left(U^{(2)}\right) = \frac{n!k!}{(n+k+1)!}, k, n = 0, 1, 2, \ldots.$$

In fact it suffices to show $\int q_1^n = \frac{1}{n+1}$. The integration over the angles ϕ_j can be combined into one ϕ, due to the rotational invariance. Write

$$q_1 = (\cos\theta_1 \cos\theta_2 + \mathrm{e}^{\mathrm{i}\phi} \sin\theta_1 \sin\theta_2)(\cos\theta_1 \cos\theta_2 + \mathrm{e}^{-\mathrm{i}\phi} \sin\theta_1 \sin\theta_2),$$

$$q_1^n = \sum_{j=0}^{n} \sum_{l=0}^{n} \binom{n}{j} \binom{n}{l} (\cos\theta_1 \cos\theta_2)^{2n-j-l} (\sin\theta_1 \sin\theta_2)^{j+l} \, \mathrm{e}^{\mathrm{i}(j-l)\phi}.$$

Now integrate with $\frac{1}{2\pi}\mathrm{d}\phi$ over $-\pi < \phi \leqslant \pi$, then over the $\mathrm{d}\theta_1 \, \mathrm{d}\theta_2$ part:

$$\begin{aligned} \int q_1^n &= 4 \sum_{j=0}^{n} \binom{n}{j}^2 \int_0^{\frac{\pi}{2}} \int_0^{\frac{\pi}{2}} (\cos\theta_1 \cos\theta_2)^{2n-2j+1} (\sin\theta_1 \sin\theta_2)^{2j+1} \, \mathrm{d}\theta_1 \, \mathrm{d}\theta_2 \\ &= \sum_{j=0}^{n} \binom{n}{j}^2 \left(\frac{(n-j)!j!}{(n+1)!} \right)^2 = \frac{1}{(n+1)^2} \sum_{j=0}^{n} 1 = \frac{1}{n+1}. \end{aligned}$$

To complete the proof

$$\begin{aligned} \int q_1^n q_2^k &= \int q_1^n (1 - q_1)^k = \sum_{j=0}^{k} \binom{k}{j} (-1)^j \int q_1^{n+j} \\ &= \sum_{j=0}^{k} \binom{k}{j} (-1)^j \frac{1}{n+j+1} = \frac{1}{n+1} \sum_{j=0}^{k} \frac{(-k)_j \, (n+1)_j}{j! \, (n+2)_j} \\ &= \frac{(n+2-n-1)_k}{(n+1) \, (n+2)_k} = \frac{n!k!}{(n+k+1)!}, \end{aligned}$$

where $(x)_j$ is the Pochhammer symbol. This used the Chu–Vandermonde sum (terminating ${}_2F_1\,(1)$) and $\frac{1}{n+1+j} = \frac{(n+1)_j}{(n+1)_j(n+1+j)} = \frac{(n+1)_j}{(n+1)(n+2)_j}$.

Appendix B. Expectation values for shadows

Consider a general matrix X acting on a $N \times N$ composite Hilbert space $\mathcal{H} = \mathcal{H}_A \otimes \mathcal{H}_B$ with entries written in a four-index notation $X_{\substack{i_1 i_2 \\ j_1 j_2}}$, where $i_1, j_1, i_2, j_2 = 1, \ldots, N$. Upper pair of indices determines the row of the matrix, while the lower pair determines its column. We use the standard operations on matrices, which in this notation read

$$X^{\dagger}_{\substack{i_1 i_2 \\ j_1 j_2}} := \overline{X}_{\substack{j_1 j_2 \\ i_1 i_2}}, \qquad \mathrm{tr}X := \sum_{i,j=1}^{N} X_{\substack{i\,j \\ i\,j}} \tag{B.1}$$

and introduce reduced matrices of size N obtained by a partial trace over a single subsystem

$$(\mathrm{tr}_A X)_{i_2 j_2} := \sum_{i=1}^{N} X_{\substack{i i_2 \\ i j_2}}, \qquad (\mathrm{tr}_B X)_{i_1 j_1} := \sum_{j=1}^{N} X_{\substack{i_1 j \\ j_1 j}}. \tag{B.2}$$

By the formula in [34] we have

$$\int_{\mathrm{U}(N)} u_{ij}\overline{u_{i'j'}}\,\mathrm{d}m\,(u) = \frac{1}{N}\delta_{ii'}\delta_{jj'}, \tag{B.3}$$

$$\begin{aligned}\int_{\mathrm{U}(N)} u_{i_1 j_1} u_{i_2 j_2}\overline{u_{i'_1 j'_1} u_{i'_2 j'_2}}\,\mathrm{d}m\,(u) &= \frac{1}{N^2-1}\left\{\delta_{i_1 i'_1}\delta_{i_2 i'_2}\delta_{j_1 j'_1}\delta_{j_2 j'_2} + \delta_{i_1 i'_2}\delta_{i_2 i'_1}\delta_{j_1 j'_2}\delta_{j_2 j'_1}\right\} \\ &\quad -\frac{1}{N(N^2-1)}\left\{\delta_{i_1 i'_1}\delta_{i_2 i'_2}\delta_{j_1 j'_2}\delta_{j_2 j'_1} + \delta_{i_1 i'_2}\delta_{i_2 i'_1}\delta_{j_1 j'_1}\delta_{j_2 j'_2}\right\},\end{aligned} \tag{B.4}$$

where $\mathrm{d}m$ denotes the Haar measure on $\mathrm{U}\,(N)$.

Let

$$z = \langle x|U \otimes VXU^{\dagger} \otimes V^{\dagger}|x\rangle, \tag{B.5}$$

where U, V are stochastically independent random unitary matrices of size N, distributed with Haar measure and $|x\rangle$ is an arbitrary vector. We are interested in obtaining mean and variance of z; thus, we will calculate $\mathbb{E}(z)$ and $\mathbb{E}(z\bar{z})$. We have

$$\mathbb{E}(z) = \mathbb{E}(\langle x|U \otimes VXU^{\dagger} \otimes V^{\dagger}|x\rangle) = \langle x|\mathbb{E}(U \otimes VXU^{\dagger} \otimes V^{\dagger})|x\rangle \tag{B.6}$$

and

$$\mathbb{E}(z\bar{z}) = \mathbb{E}(\langle x| \otimes \langle\overline{x}|(U \otimes VXU^{\dagger} \otimes V^{\dagger}) \otimes (\overline{U} \otimes \overline{V}\,\overline{X}\,U^{T} \otimes V^{T})|x\rangle \otimes |\overline{x}\rangle) \tag{B.7}$$

$$= \langle x| \otimes \langle\overline{x}|\,\mathbb{E}((U \otimes VXU^{\dagger} \otimes V^{\dagger}) \otimes (\overline{U} \otimes \overline{V}\,\overline{X}\,U^{T} \otimes V^{T}))\,|x\rangle \otimes |\overline{x}\rangle. \tag{B.8}$$

To obtain the mean we calculate

$$\mathbb{E}(U \otimes VXU^{\dagger} \otimes V^{\dagger}) = \left\{\sum_{k,l=1}^{N^2} \mathbb{E}\left((U \otimes V)_{ik} X_{kl} \overline{(U \otimes V)}_{jl}\right)\right\}_{ij} \tag{B.9}$$

$$= \left\{\sum_{k_1,k_2,l_1,l_2=1}^{N} \mathbb{E}(u_{i_1 k_1} v_{i_2 k_2} X_{\substack{k_1 k_2 \\ l_1 l_2}} \overline{u}_{j_1 l_1}\overline{v}_{j_2 l_2})\right\}_{ij} \tag{B.10}$$

$$= \left\{ \sum_{k_1,k_2,l_1,l_2=1}^{N} \frac{1}{N}\frac{1}{N}\delta_{i_1 j_1}\delta_{k_1 l_1}\delta_{i_2 j_2}\delta_{k_2 l_2} X \begin{matrix} k_1 k_2 \\ l_1 l_2 \end{matrix} \right\}_{ij} \tag{B.11}$$

$$= \frac{1}{N^2}\mathrm{tr}X\ 1_{N^2\times N^2}, \tag{B.12}$$

where we have used a convention that we split indices $\xi = N(\xi_1 - 1) + \xi_2$, and ξ_1, ξ_2 has values from $\{1, 2, \ldots N\}$. From the above, we have that for any normalized $|x\rangle$

$$\mathbb{E}(z) = \mathbb{E}(\langle x|U \otimes VXU^\dagger \otimes V^\dagger|x\rangle) = \frac{1}{N^2}\mathrm{tr}X. \tag{B.13}$$

Let us now we calculate the second moment. Let

$$M = \mathbb{E}((U \otimes VXU^\dagger \otimes V^\dagger) \otimes (\overline{U} \otimes \overline{V}\,\overline{X}U^T \otimes V^T)). \tag{B.14}$$

We have

$$\langle i_1, i_2, k_1, k_2|M|j_1, j_2, l_1, l_2\rangle \tag{B.15}$$

$$= \sum_{\alpha,\beta,\gamma,\epsilon=1}^{N^2} \mathbb{E}(u_{i_1\alpha_1} v_{i_2\alpha_2} X_{\substack{\alpha_1\alpha_2 \\ \beta_1\beta_2}} \overline{u}_{j_1\beta_1} \overline{v}_{j_2\beta_2} \overline{u}_{k_1\gamma_1} \overline{v}_{k_2\gamma_2} \overline{X}_{\substack{\gamma_1\gamma_2 \\ \epsilon_1\epsilon_2}} u_{l_1\epsilon_1} v_{l_2\epsilon_2}) \tag{B.16}$$

$$= \sum_{\alpha,\beta,\gamma,\epsilon=1}^{N^2} \mathbb{E}(u_{i_1\alpha_1} u_{l_1\epsilon_1} \overline{u}_{j_1\beta_1} \overline{u}_{k_1\gamma_1}) \mathbb{E}(v_{i_2\alpha_2} v_{l_2\epsilon_2} \overline{v}_{j_2\beta_2} \overline{v}_{k_2\gamma_2}) X_{\substack{\alpha_1\alpha_2 \\ \beta_1\beta_2}} \overline{X}_{\substack{\gamma_1\gamma_2 \\ \epsilon_1\epsilon_2}}. \tag{B.17}$$

Using formula (B.4) for the integral we have that $M = c_1 M^{(1)} + c_2 M^{(2)} + c_3 M^{(3)} + c_4 M^{(4)}$, where

$$M^{(1)} = \sum_{i_1,i_2,k_1,k_2=1}^{N} |i_1, i_2, k_1, k_2\rangle\langle i_1, i_2, k_1, k_2|,$$

$$\begin{aligned} c_1 &= \frac{1}{(N^2-1)^2} \sum_{\alpha,\beta,\gamma,\epsilon=1}^{N^2} \left(\delta_{\alpha_1\beta_1}\delta_{\epsilon_1\gamma_1} - \frac{1}{N}\delta_{\alpha_1\gamma_1}\delta_{\beta_1\epsilon_1}\right)\left(\delta_{\alpha_2\beta_2}\delta_{\epsilon_2\gamma_2} - \frac{1}{N}\delta_{\alpha_2\gamma_2}\delta_{\beta_2\epsilon_2}\right) X_{\substack{\alpha_1\alpha_2 \\ \beta_1\beta_2}} \overline{X}_{\substack{\gamma_1\gamma_2 \\ \epsilon_1\epsilon_2}} \\ &= \frac{1}{(N^2-1)^2}\left(\sum_{\alpha_1,\alpha_2,\gamma_1,\gamma_2=1}^{N} X_{\substack{\alpha_1\alpha_2 \\ \alpha_1\alpha_2}} \overline{X}_{\substack{\gamma_1\gamma_2 \\ \gamma_1\gamma_2}} - \frac{1}{N} \sum_{\alpha_1,\alpha_2,\beta_2,\gamma_1=1}^{N} X_{\substack{\alpha_1\alpha_2 \\ \alpha_1\beta_2}} \overline{X}_{\substack{\gamma_1\alpha_2 \\ \gamma_1\beta_2}} \right. \\ &\quad \left. - \frac{1}{N} \sum_{\alpha_1,\alpha_2,\beta_1,\gamma_2=1}^{N} X_{\substack{\alpha_1\alpha_2 \\ \beta_1\alpha_2}} \overline{X}_{\substack{\alpha_1\gamma_2 \\ \beta_1\gamma_2}} + \frac{1}{N^2} \sum_{\alpha_1,\alpha_2,\beta_1,\beta_2=1}^{N} X_{\substack{\alpha_1\alpha_2 \\ \beta_1\beta_2}} \overline{X}_{\substack{\alpha_1\alpha_2 \\ \beta_1\beta_2}} \right) \\ &= \frac{1}{(N^2-1)^2}\left(\mathrm{tr}(X)\mathrm{tr}(X^\dagger) - \frac{1}{N}\mathrm{tr}(\mathrm{tr}_A(X)\mathrm{tr}_A(X)^\dagger) - \frac{1}{N}\mathrm{tr}(\mathrm{tr}_B(X)\mathrm{tr}_B(X)^\dagger) + \frac{1}{N^2}\mathrm{tr}(XX^\dagger)\right) \\ &= \frac{1}{(N^2-1)^2}\left(|\mathrm{tr}X|^2 - \frac{1}{N}\|\mathrm{tr}_A(X)\|_{\mathrm{HS}}^2 - \frac{1}{N}\|\mathrm{tr}_B(X)\|_{\mathrm{HS}}^2 + \frac{1}{N^2}\|X\|_{\mathrm{HS}}^2\right). \end{aligned} \tag{B.18}$$

Similarly

$$M^{(2)} = \sum_{i_1,i_2,j_1,k_2=1}^{N} |j_1, i_2, j_1, k_2\rangle\langle i_1, i_2, i_1, k_2|,$$

$$c_2 = \frac{1}{(N^2-1)^2} \sum_{\alpha,\beta,\gamma,\epsilon=1}^{N^2} \left(\delta_{\alpha_1\gamma_1}\delta_{\beta_1\epsilon_1} - \frac{1}{N}\delta_{\alpha_1\beta_1}\delta_{\epsilon_1\gamma_1}\right)\left(\delta_{\alpha_2\beta_2}\delta_{\epsilon_2\gamma_2} - \frac{1}{N}\delta_{\alpha_2,\gamma_2}\delta_{\beta_2,\epsilon_2}\right) X_{\substack{\alpha_1\alpha_2\\ \beta_1\beta_2}} \overline{X}_{\substack{\gamma_1\gamma_2\\ \epsilon_1\epsilon_2}}$$
$$= \frac{1}{(N^2-1)^2}\left(\|\mathrm{tr}_B(X)\|_{\mathrm{HS}}^2 - \frac{1}{N}\|X\|_{\mathrm{HS}}^2 - \frac{1}{N}|\mathrm{tr}X|^2 + \frac{1}{N^2}\|\mathrm{tr}_A(X)\|_{\mathrm{HS}}^2\right). \tag{B.19}$$

Next we have

$$M^{(3)} = \sum_{i_1,i_2,j_2,k_1=1}^{N} |i_1, j_2, k_1, j_2\rangle\langle i_1, i_2, k_1, i_2|,$$
$$c_3 = \frac{1}{(N^2-1)^2}\left(\|\mathrm{tr}_A(X)\|_{\mathrm{HS}}^2 - \frac{1}{N}\|X\|_{\mathrm{HS}}^2 - \frac{1}{N}|\mathrm{tr}X|^2 + \frac{1}{N^2}\|\mathrm{tr}_B(X)\|_{\mathrm{HS}}^2\right). \tag{B.20}$$

Finally

$$M^{(4)} = \sum_{i_1,i_2,j_i,j_2=1}^{N} |j_1, j_2, j_1, j_2\rangle\langle i_1, i_2, i_1, i_2|,$$
$$c_4 = \frac{1}{(N^2-1)^2}\left(\|\mathrm{tr}_B(X)\|_{\mathrm{HS}}^2 - \frac{1}{N}\|\mathrm{tr}_A(X)\|_{\mathrm{HS}}^2 - \frac{1}{N}\|\mathrm{tr}_B(X)\|_{\mathrm{HS}}^2 + \frac{1}{N^2}|\mathrm{tr}X|^2\right). \tag{B.21}$$

The integrals of the above type, for a fixed dimension, can be calculated with the use of computer algebra program `IntU` [37].

Appendix C. Variance values for shadows with fixed Schmidt numbers

Let us consider any pure state $|x\rangle$ from the $N \times N$ composite Hilbert space $\mathcal{H} = \mathcal{H}_A \otimes \mathcal{H}_B$ with fixed Schmidt numbers $\lambda_1, \lambda_2, \ldots, \lambda_N$; thus, we have

$$|x\rangle = \sum_{i=1}^{N} \sqrt{\lambda_i}|i^A\rangle \otimes |i^B\rangle, \tag{C.1}$$

for some orthogonal bases $|i^A\rangle$, $|i^B\rangle$. For simplicity we can take computational bases. We have the following identities:

$$\langle x| \otimes \langle \overline{x}|M_1|x\rangle \otimes |\overline{x}\rangle = \langle x| \otimes \langle \overline{x}|M_4|x\rangle \otimes |\overline{x}\rangle = 1 \tag{C.2}$$

$$\langle x| \otimes \langle \overline{x}|M_2|x\rangle \otimes |\overline{x}\rangle = \langle x| \otimes \langle \overline{x}|M_3|x\rangle \otimes |\overline{x}\rangle = \sum_{i=1}^{N} \lambda_i^2. \tag{C.3}$$

Thus we have

$$\langle x| \otimes \langle \overline{x}|M|x\rangle \otimes |\overline{x}\rangle = c_1 + c_4 + (c_2 + c_3)\sum_{i=1}^{N} \lambda_i^2. \tag{C.4}$$

Note that the above depends only on a purity of reduced state. In the case of maximally entangled state ($\lambda_i = \frac{1}{N}$ for $i = 1, 2, \ldots N$), the second moment is given by

$$\langle x| \otimes \langle \overline{x}|M|x\rangle \otimes |\overline{x}\rangle \tag{C.5}$$
$$= \frac{1}{N^2(N^2-1)}\left(|\mathrm{tr}X|^2 + \|X\|_{\mathrm{HS}}^2\right) - \frac{1}{N^3(N^2-1)}\left(\|\mathrm{tr}_A(X)\|_{\mathrm{HS}}^2 + \|\mathrm{tr}_B(X)\|_{\mathrm{HS}}^2\right). \tag{C.6}$$

The above implies the result (25) for the variance with respect to the entangled shadow.

In the case of separable states ($\lambda_i = \delta_{1,i}$ for $i = 1, 2, \ldots N$), we obtain

$$\langle x| \otimes \langle \bar{x}|M|x\rangle \otimes |\bar{x}\rangle \tag{C.7}$$

$$= \frac{1}{N^2(N+1)^2}\left(|\mathrm{tr}X|^2 + \|\mathrm{tr}_A(X)\|_{\mathrm{HS}}^2 + \|\mathrm{tr}_B(X)\|_{\mathrm{HS}}^2 + \|X\|_{\mathrm{HS}}^2\right), \tag{C.8}$$

which implies the result (20) for the variance with respect to the separable shadow.

References

[1] Horodecki R, Horodecki P, Horodecki M and Horodecki K 2009 Quantum entanglement *Rev. Mod. Phys.* **81** 865–942

[2] Kuś M and Życzkowski K 2001 Geometry of entangled states *Phys. Rev.* A **63** 032307

[3] Mosseri R and Dandoloff R 2001 Geometry of entangled states, Bloch spheres and Hopf fibrations *J. Phys. A: Math. Gen.* **34** 10243–52

[4] Verstraete F, Dehaene J and De Moor B 2002 On the geometry of entangled states *J. Mod. Opt.* **49** 1277–87

[5] Levay P 2004 The geometry of entanglement: metrics, connections and the geometric phase *J. Phys. A: Math. Gen.* **37** 1821–42

[6] Avron J E and Kenneth O 2009 Entanglement and the geometry of two qubit *Ann. Phys., NY* **324** 470–96

[7] Bertlmann R and Krammer P 2009 Entanglement witnesses and geometry of entanglement of two-qutrit states *Ann. Phys., NY* **324** 1388–407

[8] Bengtsson I and Życzkowski K 2006 *Geometry of Quantum States* (Cambridge: Cambridge University Press)

[9] Brody D C, Gustavsson A C T and Hughston L P 2007 Entanglement of three-qubit geometry *J. Phys.: Conf. Ser.* **67** 012044

[10] Sawicki A, Huckleberry A and Kuś M 2011 Symplectic geometry of entanglement *Commun. Math. Phys.* **305** 441–68

[11] Vedral V 2007 *Introduction to Quantum Information Science* (Oxford: Oxford University Press)

[12] Petz D 2008 *Quantum Information Theory and Quantum Statistics* (Berlin: Springer)

[13] Sinołęcka M, Życzkowski K and Kuś M 2002 Manifolds of equal entanglement for composite quantum systems *Acta Phys. Pol.* B **33** 2081–95

[14] Horn R A and Johnson C R 1994 *Topics in Matrix Analysis* (Cambridge: Cambridge University Press)

[15] Gustafson K E and Rao D K M 1997 *Numerical Range: The Field of Values of Linear Operators and Matrices* (New York: Springer)

[16] Gutkin E 2004 The Toeplitz–Hausdorff theorem revisited: relating linear algebra and geometry *Math. Intell.* **26** 8–14

[17] Jonckheere E, Ahmad F and Gutkin E 1998 Differential topology of numerical range *Linear Algebra Appl.* **279** 227–54

[18] Henrion D 2010 Semidefinite geometry of the numerical range *Electron. J. Linear Algebra* **20** 322–32

[19] Schulte-Herbrüggen T, Dirr G, Helmke U and Glaser S J 2008 The significance of the *c*-numerical range and the local *c*-numerical range in quantum control and quantum information *Linear Multilinear Algebra* **56** 3–26

[20] Kribs D W, Pasieka A, Laforest M, Ryan C and Silva M P 2009 Research problems on numerical ranges in quantum computing *Linear Multilinear Algebra* **57** 491–502

[21] Gawron P, Puchała Z, Miszczak J A, Skowronek Ł, Choi M-D and Życzkowski K 2010 Restricted numerical range: a versatile tool in the theory of quantum information *J. Math. Phys.* **51** 102204

[22] Marcus M and Wang B 1980 Some variations on the numerical range *Linear Multilinear Algebra* **9** 111–20

[23] Bebiano N, Li C K and da Providencia J 1991 The numerical range and decomposable numerical range of matrices *Linear Multilinear Algebra* **29** 195–205

[24] Dirr G, Helmke U, Kleinsteuber M and Schulte-Herbrüggen T 2008 Relative *c*-numerical ranges for applications in quantum control and quantum information *Linear Multilinear Algebra* **56** 27–51

[25] Puchała Z, Gawron P, Miszczak J A, Skowronek Ł, Choi M-D and Życzkowski K 2010 Product numerical range in a space with tensor product structure *Linear Algebra Appl.* **434** 3274–342

[26] Dunkl C F, Gawron P, Holbrook J A, Puchała Z and Życzkowski K 2011 Numerical shadows: measures and densities on the numerical range *Linear Algebra Appl.* **434** 2042–80

[27] Gallay T and Serre D 2010 The numerical measure of a complex matrix arXiv:1009.1522

[28] Dunkl C F, Gawron P, Holbrook J A, Miszczak J, Puchała Z and Życzkowski K 2011 Numerical shadow and geometry of quantum states *J. Phys. A: Math. Theor.* **44** 335301 (arXiv:1104.2760)

[29] Caves C M, Fuchs C A and Rungta P 2001 Entanglement of formation of an arbitrary state of two rebits *Found. Phys. Lett.* **14** 199–212
[30] Choi M-D, Kribs D W and Życzkowski K 2006 Higher-rank numerical ranges and compression problems *Linear Algebra Appl.* **418** 828–39
[31] Choi M-D, Holbrook J A, Kribs D W and Życzkowski K 2007 Higher-rank numerical ranges of unitary and normal matrices *Oper. Matrices* **1** 409–26
[32] Bengtsson I, Ericsson A, Kuś M, Tadej W and Życzkowski K 2005 Birkhoff's polytope and unistochastic matrices, $N = 3$ and $N = 4$ *Commun. Math. Phys.* **259** 307–24
[33] Dunkl C and Życzkowski K 2009 Volume of the set of unistochastic matrices of order 3 and the mean Jarlskog invariant *J. Math. Phys.* **50** 123521
[34] Collins B and Śniady P 2006 Integration with respect to the Haar measure on unitary, orthogonal and symplectic group *Commun. Math. Phys.* **264** 773–95
[35] Dür W, Vidal G and Cirac J I 2000 Three qubits can be entangled in two inequivalent ways *Phys. Rev.* A **62** 062314
[36] Provost S B and Cheong Y H 2000 On the distribution of linear combinations of the components of a Dirichlet random vector *Can. J. Stat.* **28** 417–25
[37] Puchała Z and Miszczak J A 2011 Symbolic integration with respect to the Haar measure on the unitary group in Mathematica arXiv:1109.4244
[38] Bailey W N 1935 *Generalized Hypergeometric Series* (London: Cambridge University Press)
[39] Dunkl C F 1995 Intertwining operators associated to the group S_3 *Trans. Am. Math. Soc.* **347** 3347–74
[40] Życzkowski K, Horodecki P, Horodecki M and Horodecki R 2001 Dynamics of quantum entanglement *Phys. Rev.* A **65** 012101
[41] Yu T and Eberly J H 2004 Finite-time disentanglement via spontaneous emission *Phys. Rev. Lett.* **93** 140404
[42] Yu T and Eberly J H 2009 Sudden death of entanglement *Science* **323** 598–601
[43] Mintert F, Carvalho A R R, Kuś M and Buchleitner A 2005 Measures and dynamics of entangled states *Phys. Rep.* **415** 207–59
[44] Ficek Z and Tanaś R 2006 Dark periods and revivals of entanglement in a two-qubit system *Phys. Rev.* A **74** 024304
[45] Derkacz Ł and Jakobczyk L 2006 Quantum interference and evolution of entanglement in a system of three-level atoms *Phys. Rev.* A **74** 032313
[46] Dajka J and Łuczka J 2008 Origination and survival of qudit–qudit entanglement in open systems *Phys. Rev.* A **77** 062303
[47] Ficek Z and Tanaś R 2008 Delayed sudden birth of entanglement *Phys. Rev.* A **77** 054301